

Adaptive Experimental Design Using Shrinkage Estimators

Evan T. R. Rosenman

Department of Mathematical Sciences
Claremont McKenna College
Claremont, CA, United States

Kristen B. Hunter

School of Mathematics and Statistics
University of New South Wales
Sydney, New South Wales, Australia

February 10, 2026

Abstract

In the setting of multi-armed trials, adaptive designs are a popular way to increase estimation efficiency, identify optimal treatments, or maximize rewards to individuals. Recent work has considered the case of estimating the effects of K active treatments, relative to a control arm, in a sequential trial. Several papers have proposed sequential versions of the classical Neyman allocation scheme to assign treatments as individuals arrive, typically with the goal of using Horvitz-Thompson-style estimators to obtain causal estimates at the end of the trial. However, this approach may be inefficient in that it fails to borrow information across the treatment arms.

In this paper, we consider adaptivity when the final causal estimation is obtained using a Stein-like shrinkage estimator for heteroscedastic data. Such an estimator shares information across treatment effect estimates, providing provable reductions in expected squared error loss relative to estimating each causal effect in isolation. Moreover, we show that the expected loss of the shrinkage estimator takes the form of a Gaussian quadratic form, allowing it to be computed efficiently using numerical integration. This result paves the way for sequential adaptivity, allowing treatments to be assigned to minimize the shrinker loss. Through simulations, we demonstrate that this approach can yield meaningful reductions in estimation error. We also characterize how our adaptive algorithm assigns treatments differently than would a sequential Neyman allocation.

Contents

1	Introduction	2
2	Literature Review	2
3	SURE and Candidate Estimators	4
3.1	Notation and Assumptions	4
3.2	Difference-in-Means Estimator	4
3.3	Stein's Unbiased Risk Estimate	5
3.4	Candidate Estimators	6
4	Oracle Designs	7
4.1	A Modified Neyman Allocation	7
4.2	Minimizers in the Low Signal-to-Noise Ratio Regime	7
4.2.1	Bock's Estimator	8
4.2.2	SURE-Min Estimator	9
4.2.3	Dimmery's Estimator	10
4.3	Simulated Static Allocations	11
4.3.1	Computing Risk-Minimizing Allocations	11
4.3.2	Simulation Setup	11
4.3.3	Simulation Results	12

5 Adaptive Risk Minimization	13
5.1 Efficient Risk Computation	14
5.2 Greedy Algorithm	15
5.3 Simulations	16
6 Discussion	18

1 Introduction

Adaptive experimental designs offer a powerful tool to improve experimentation. In such designs, the treatment assignment rule used for new arrivals is updated based on the outcomes already observed. These updates can be targeted toward improving the efficiency of estimating causal contrasts (Dai et al., 2023), more rapidly identifying optimal treatments (Villar et al., 2015), or maximizing the utility of individuals in the trial (Rosenberger et al., 2001).

We consider the first such objective in the context of a multi-armed randomized experiment in which there are K possible active treatment levels, as well as a control treatment level. We suppose the trial is “online” in the sense that individuals arrive sequentially and, upon arrival, must be assigned to a treatment status $k \in \{0, \dots, K\}$, where $k = 0$ denotes the control and $k = 1, \dots, K$ denote the active treatments.

We assume that trial participants are randomly sampled from an infinite super-population. For each individual in this super-population, we define potential outcomes $Y(k)$ corresponding to every possible treatment assignment. The causal quantities of interest are the average treatment effects

$$\tau_k = \mathbb{E}(Y(k) - Y(0)), \quad k = 1, \dots, K,$$

where the expectation is taken with respect to the super-population distribution of potential outcomes. We collect these parameters into a vector $\tau = (\tau_1, \dots, \tau_K) \in \mathbb{R}^K$. Throughout, we assume standard conditions, such as SUTVA, and for simplicity we do not incorporate covariates.

A central challenge in adaptive experiments is the design of treatment assignment rules that best exploit the accumulating data. The Neyman allocation (Neyman, 1934), a classical and much-vaunted sampling result, suggests allocating units to treatments in proportion to their potential outcome standard deviations. Recent work has extended this idea to sequential and adaptive settings (Dai et al., 2023; Zhao, 2023; Chen et al., 2025), proposing online versions of Neyman-style allocation schemes in which treatment probabilities are updated as outcome data accrue. These approaches are often paired with Horvitz-Thompson-style estimators to retain unbiasedness under adaptive assignment.

Such methods may be suboptimal when the goal is to estimate all of the treatment effects simultaneously. In particular, the treatment effects are often related and can beneficially share information. Shrinkage estimators provide a principled way to borrow strength across effect estimates and can achieve lower expected squared error loss than estimating each effect separately, even in heteroscedastic settings.

In this manuscript, we study adaptive experimental design when final inference is conducted using a Stein-like shrinkage estimator for the vector of treatment effects. Under standard approximate Gaussian distributions for the arm-level estimators, the expected squared error loss of such shrinkage estimators can be written as a Gaussian quadratic form. This representation allows the risk to be computed efficiently using numerical integration, making it feasible to design adaptive assignment rules that directly target minimization of the shrinkage risk.

The remainder of this paper proceeds as follows. Section 2 reviews the relevant literature on Neyman allocation and adaptive designs. Section 3 introduces three candidate shrinkage estimators and explains how their risk can be estimated via an adaptation of Stein’s Unbiased Risk Estimate (Stein, 1981). Section 4 considers oracle designs in the case where the potential outcome means and variances are known for each treatment arm. We begin by solving for the Neyman allocation, and then consider the risk-minimizing allocations for each of the candidate shrinkers. Section 5 introduces our greedy adaptivity scheme, demonstrating how shrinker risk can be efficiently computed via numerical integration. Subsequent simulations evince the benefits of adaptivity in practice. Section 6 concludes.

2 Literature Review

Adaptive experimental designs can vary widely in their objectives. One fundamental distinction is between designs that prioritize identifying and exploiting the best treatment and those that prioritize

precise estimation of causal effects. All adaptive designs make a tradeoff between exploration and exploitation. Sometimes this tradeoff is explicitly optimized, such as in Thompson sampling; other methods deal with this tradeoff by having a warm-up period.

In a multi-armed bandit setting, the primary goal is to maximize the expected reward. The reward is maximized by quickly identifying the best-performing arm, so that the largest possible number of units are assigned to it. A canonical approach is Thompson sampling, which randomly assigns units to arms proportional to the posterior probability that each arm is optimal (Thompson, 1933; Agrawal and Goyal, 2012; Russo et al., 2018). More recent work has considered a “top-two” variant of Thompson sampling, where more aggressive exploration is induced by randomizing within the two arms that appear most promising based on the posterior (Russo, 2016; Kasy and Sautmann, 2021; Rosenzweig and Offer-Westort, 0). Dimmery et al. (2019) shows that empirical Bayes shrinkage can be applied to produce results similar to “top-two Thomson sampling”, but with better performance in selecting a set of best arms rather than just the top two.

Unlike traditional randomized trials, bandit designs do not typically include a control arm, and the emphasis is not on precise estimation of effect sizes. Instead, the aim is to minimize cumulative regret by rapidly exploiting the reward-maximizing treatment option. As a simple example, consider an A/B test in which a company seeks to determine which color of a website search bar – red or blue – maximizes revenue. The company does not care about pairwise comparisons between colors, nor about estimating revenue levels with high precision. Even if the improvement from red over blue is small, red would be chosen if it yields the highest expected profit. Accordingly, the firm wishes to minimize exposure to inferior designs during the experiment, rather than to learn finely grained effect sizes.

By contrast, efficiency-oriented adaptive designs aim to estimate causal effects as precisely as possible. Here, the treatment allocation is chosen to minimize the variance of treatment effect estimators, often under a fixed total sample size. In this setting, trials typically include a control arm, and treatment effects are defined relative to that control. The success of the design is evaluated by the aggregate precision of the effect estimates.

For example, consider a clinical trial comparing three new drugs to a standard treatment. The goal is not simply to identify which drug performs best, but to estimate each drug’s causal effect relative to the control with high precision. A drug that is superior, but yields only a marginal clinical benefit, may not be worth pursuing. Similarly, cost, side effects, or scalability considerations may dominate small differences in efficacy. In such settings, precise effect estimation – not just best-arm identification – is essential.

Though originally derived as an optimal strategy for stratified sampling, the Neyman allocation is a canonical efficiency-oriented design, minimizing the statistical risk of a simple difference-in-means estimator. Optimal assignment probabilities are proportional to arm-specific potential outcome standard deviations (Neyman, 1934; Blackwell and Hodges, 1979; Atkinson, 1982). Because these quantities are unknown at the outset of an adaptive experiment, various papers have proposed schemes to approximate these quantities and update treatment probabilities accordingly. Blackwell et al. (2022) proposes approximating these quantities with a pilot batch, but Cai and Rafi (2024) notes that this approach can yield higher asymptotic variance than a non-adaptive approach when the pilot is small. Other methods consider multistage (Zhao, 2023) and online (Dai et al., 2023; Chen et al., 2025) variants.

When covariates are observed prior to treatment assignment, adaptive designs can be further enhanced to improve efficiency. A standard approach is to estimate arm-specific variances conditional on covariate values or strata. Hahn et al. (2011) proposes implementing a Neyman allocation conditional on covariates by estimating outcome variances within treatment and control groups. Tabord-Meehan (2018) studies a two-stage randomized controlled trial in which strata are learned rather than prespecified. He proposed using pilot data to estimate a stratification via tree-based methods, and selecting stratum-specific allocations via a Neyman-like approach. Li and Owen (2024) characterize optimal allocation rules that minimize the asymptotic variance of treatment effect estimators under general covariate-adaptive designs, providing theoretical guarantees for efficiency gains relative to classical randomization schemes. Moreover, in the presence of covariates, alternative objectives are also possible. For example, Arbour et al. (2022) introduces a method based on weighted online discrepancy minimization in multiarm trials. Here, the goal is to achieve covariate balance across arms, rather than explicitly improving estimation precision.

Hybrid objectives are also common. In many applications, investigators wish to exploit superior treatments while retaining enough control observations to enable stable and interpretable effect estimation. Offer-Westort et al. (2021) propose Control-Augmented Thompson Sampling, which modifies standard Thompson sampling so that the control arm’s sample size tracks that of the currently best-performing treatment. Similarly, Trippa et al. (2012) develop a Bayesian adaptive algorithm for multi-armed sur-

vival trials that balances patient benefit with reliable control comparisons. Related work explores optimal trade-offs between regret minimization and estimation precision in adaptive trials (Wason and Trippa, 2014; Villar et al., 2015).

Another key design choice concerns whether the experiment is run for a fixed sample size or governed by a stopping rule. Adaptive trials may terminate early if one arm is shown to be sufficiently superior, or if continuing the experiment is deemed unlikely to change the decision. While early stopping can substantially reduce cost or ethical burden, it complicates statistical inference, as conventional estimators and confidence intervals may no longer be valid (Johari et al., 2017). A growing literature studies both optimal stopping rules and valid post-selection inference in adaptive experiments (Ham et al., 2023).

Our goal in this manuscript is to develop an adaptive allocation rule tailored to shrinkage-based estimation of multi-armed treatment effects. We assume the final analysis will use a Stein-like estimator that borrows strength across the K treatment effect estimates. The allocation method then differs from most efficiency-oriented adaptive designs, which typically seek to minimize the variance of unbiased difference-in-means or Horvitz-Thompson-style estimators. This shift changes the design problem: assignment decisions should be evaluated by their impact on the risk of the shrinkage estimator, not by the marginal variance of each arm in isolation.

To make this method feasible in an online trial, we show that, for a broad class of shrinkers, the expected squared-error risk can be written as a linear combination of expectations of ratios of Gaussian quadratic forms, which can be computed efficiently via one-dimensional numerical integration. This result yields a practical sequential algorithm that, at each enrollment, assigns the arriving unit to the arm that minimizes the estimated shrinkage risk under a plug-in model for the currently best estimate of the treatment effects and their covariance matrix. In simulations, we study when shrinkage estimators dominate the difference-in-means benchmark and how the resulting risk-minimizing allocations differ from sequential Neyman-style rules.

3 SURE and Candidate Estimators

3.1 Notation and Assumptions

At completion, suppose we have N total individuals who have been enrolled in the trial, with individuals indexed by $i = 1, \dots, N$. Denote by $W_i \in \{0, 1, \dots, K\}$ the treatment assigned to individual i , and define

$$n_k = \sum_{i=1}^N \mathbb{I}(W_i = k), \quad k = 0, \dots, K$$

as the number of units assigned to treatment k .

As discussed in Section 1, we operate in the potential outcomes framework (Rubin, 1974), and assume units are sampled i.i.d. from a super-population. We also make the standard Stable Unit Treatment Value Assumption (SUTVA; Rubin, 1980), such that we observe outcomes

$$Y_i = Y_i(W_i), \quad i = 1, \dots, N,$$

for each individual i .

We also need some notation to define means and variances of potential outcomes. We use the notation

$$\mu_k = \mathbb{E}(Y(k)) \quad \text{and} \quad V_k = \text{var}(Y(k)),$$

for $k = 0, \dots, K$, where the expectation and variance here are again over the population from which the experimental units are sampled. Under our definitions, we can also write

$$\tau_k = \mu_k - \mu_0, \quad k = 1, \dots, K.$$

3.2 Difference-in-Means Estimator

The simplest choice of estimator is $\hat{\tau} = (\hat{\tau}_1, \dots, \hat{\tau}_K)$ where

$$\hat{\tau}_k = \frac{1}{n_k} \sum_{i=1}^n Y_i \cdot \mathbb{I}(W_i = k) - \frac{1}{n_0} \sum_{i=1}^n Y_i \cdot \mathbb{I}(W_i = 0).$$

This difference-in-means estimator is unbiased, i.e.

$$\mathbb{E}(\hat{\tau}) = \tau.$$

We can also characterize the variance of each component as

$$\sigma_k^2 \equiv \text{var}(\hat{\tau}_k) = \frac{V_k}{n_k} + \frac{V_0}{n_0}.$$

The entries of $\hat{\tau}$ will *not* be independent of one another, since each depends on the estimate from the control arm. It is straightforward to show that

$$\text{cov}(\hat{\tau}_j, \hat{\tau}_k) = \frac{V_0}{n_0}, \quad \text{for } j \neq k.$$

We can invoke a Central Limit Theorem on the entries of $\hat{\tau}$ as long as the potential outcomes $Y(k)$ are bounded and we have obtained a reasonably large number of samples in each arm. Recent work (see e.g. Hadad et al., 2021) has highlighted that adaptivity can undermine asymptotic normality if treatment selection is too responsive to estimated responses under each treatment. For clarity of exposition, we explicitly assume this is not the case, and suppose adaptivity is not so aggressive as to undermine the CLT. Thus, approximately,

$$\hat{\tau} \sim \mathcal{N}(\boldsymbol{\tau}, \boldsymbol{\Sigma}) \quad \text{where} \quad \boldsymbol{\Sigma} = \begin{pmatrix} \frac{V_1}{n_1} + \frac{V_0}{n_0} & \frac{V_0}{n_0} & \cdots & \frac{V_0}{n_0} \\ \frac{V_0}{n_0} & \frac{V_2}{n_2} + \frac{V_0}{n_0} & \cdots & \frac{V_0}{n_0} \\ \vdots & \vdots & \ddots & \vdots \\ \frac{V_0}{n_0} & \frac{V_0}{n_0} & \cdots & \frac{V_K}{n_K} + \frac{V_0}{n_0} \end{pmatrix}.$$

3.3 Stein's Unbiased Risk Estimate

It is well known that in parallel estimation problems like the one described, researchers can achieve reductions in statistical risk by using some form of shrinkage estimation. The key idea is to introduce a small amount of bias by “shrinking” the estimates toward a fixed point or toward their mean. The compensatory reduction in variance due to the shrinkage is such that one achieves a lower statistical risk than with an unbiased estimator.

The most classic estimator of this type is the James-Stein estimator (Stein, 1956), which shrinks an estimate of a multivariate normal mean vector towards zero. Though we assume approximate normality of $\hat{\tau}$, the classical James-Stein estimator is inappropriate for our setting, because its construction assumes the data are homoscedastic and that the entries are independent.

There are a number of different adaptations of the James-Stein estimator to the settings of heteroscedasticity and dependence (see e.g. Xie et al., 2012a; Dimmery et al., 2019). Before considering the precise form of our adapted estimator, we introduce a useful tool for construction and evaluation of shrinkage estimators: Stein's Unbiased Risk Estimate (Stein, 1981). The precise statement is given below.

Lemma 1 (SURE). *Suppose $\mathbf{X} \sim \mathcal{N}(\boldsymbol{\mu}, \boldsymbol{\Sigma}) \in \mathbb{R}^K$ for non-degenerate $\boldsymbol{\Sigma} \in \mathbb{R}^{K \times K}$. We consider an estimator of $\boldsymbol{\mu} \in \mathbb{R}^K$ of the form*

$$\hat{\delta}(\mathbf{X}) = \mathbf{X} - g(\mathbf{X}),$$

for $g(\cdot)$ differentiable and L_2 integrable.

Define $\mathcal{J}_g(\mathbf{X})$ as the Jacobian matrix of $g(\cdot)$ evaluated at \mathbf{X} . Then, for loss function $\mathcal{L}(\boldsymbol{\mu}, \mathbf{v}) = \mathbb{E}(\|\boldsymbol{\mu} - \mathbf{v}\|_2^2)$, we have

$$\mathbb{E}(\mathcal{L}(\hat{\delta}(\mathbf{X}), \boldsymbol{\mu})) = \text{tr}(\boldsymbol{\Sigma}) + \mathbb{E}\left(\|g(\mathbf{X})\|_2^2 - 2 \cdot \text{tr}(\boldsymbol{\Sigma} \mathcal{J}_g(\mathbf{X}))\right). \quad (1)$$

Hence, the estimator

$$\text{SURE}(\hat{\delta}(\mathbf{X})) = \text{tr}(\boldsymbol{\Sigma}) + \|g(\mathbf{X})\|_2^2 - 2 \cdot \text{tr}(\boldsymbol{\Sigma} \mathcal{J}_g(\mathbf{X})) \quad (2)$$

is unbiased for the risk $\mathbb{E}(\mathcal{L}(\hat{\delta}(\mathbf{X}), \boldsymbol{\mu}))$.

Proof. See the Appendix, Section A.

3.4 Candidate Estimators

We consider several candidate shrinkage estimators to apply to the difference-in-means estimator $\hat{\tau}$. All of these candidates will work with our adaptive treatment allocation method.

Bock's estimator. The first candidate is the shrinker of Bock (1975), which is explicitly designed to work with Gaussian vectors with dependent entries. Denoting as $\lambda_{\max}(\Sigma)$ the largest eigenvalue of Σ , the estimator is given by

$$\hat{\delta}_B = \left(1 - \frac{\tilde{p} - 2}{\hat{\tau}^\top \Sigma^{-1} \hat{\tau}}\right) \hat{\tau} \quad \text{where} \quad \tilde{p} = \frac{\text{tr}(\Sigma)}{\lambda_{\max}(\Sigma)}.$$

Note that $0 \leq \tilde{p} \leq K$. Bock showed that the estimator dominates $\hat{\tau}$ if $\text{tr}(\Sigma) > 2\lambda_{\max}(\Sigma)$. The estimator is attractive for its simplicity, and will be used as our primary motivating example.

SURE-Min estimator. An alternative estimator can be obtained by directly minimizing Stein's Unbiased Risk Estimate (Equation 2), a tradition with a long history in the statistics literature (see e.g. Li et al., 1985; Xie et al., 2012a). We consider the class of all estimators which shrink $\hat{\tau}$ toward zero by a constant factor $\lambda \in \mathbb{R}$, i.e. estimators of the form

$$\hat{\delta}(\hat{\tau}) = (1 - \lambda)\hat{\tau}.$$

An unbiased estimate of the risk of such an estimator is

$$\text{SURE}(\hat{\delta}(\hat{\tau})) = \text{tr}(\Sigma) + \lambda^2 \|\hat{\tau}\|_2^2 - 2\lambda \cdot \text{tr}(\Sigma),$$

which has minimizer $\lambda = \text{tr}(\Sigma)/\|\hat{\tau}\|_2^2$. Thus, we define our second candidate estimator as

$$\hat{\delta}_S = \left(1 - \frac{\text{tr}(\Sigma)}{\|\hat{\tau}\|_2^2}\right) \hat{\tau},$$

where $\|\hat{\tau}\|_2^2 = \sum_k \hat{\tau}_k^2$. We can again use Lemma 1 to establish a condition under which $\hat{\delta}_S$ dominates $\hat{\tau}$.

Lemma 2. $\hat{\delta}_S$ dominates $\hat{\tau}$ if

$$4 \cdot \lambda_{\max}(\Sigma) < \text{tr}(\Sigma).$$

Proof. See the Appendix, Section B.

Dimmery's estimator. A final alternative is a modified version of the estimator proposed in Dimmery et al. (2019). Dimmery and co-authors consider the setting of online experiments, in which their objective is to estimate the mean response under each treatment. They use a heteroscedastic version of the James-Stein estimator that shrinks toward the grand mean. Because we are considering contrasts between the mean response under each treatment and the mean response under a control, we modify the estimator to shrink toward 0 instead. We refer to this estimator as $\hat{\delta}_D$, whose entries are given by

$$\hat{\delta}_{D,k} = \left(1 - \frac{(K-2)\sigma_k^2}{\|\hat{\tau}\|_2^2}\right) \hat{\tau}_k, \quad k = 1, \dots, K.$$

We can use Lemma 1 to establish the following condition, under which the risk of $\hat{\delta}_D$ is strictly less than that of $\hat{\tau}$ regardless of the true value of τ .

Lemma 3. $\hat{\delta}_D$ dominates $\hat{\tau}$ if

$$\frac{1}{2} \left(\max_k \sigma_k^2 \right) \left((K-2)(\max_k \sigma_k^2) + 4\lambda_{\max}(\Sigma) \right) \leq \sum_k \sigma_k^4. \quad (3)$$

Proof. See the Appendix, Section C.

As with the maximum eigenvalue condition for Bock's estimator, Lemmas 2 and 3 are useful for practitioners in that they provide a condition that can be checked at the end of the online trial to obtain a guarantee that the risk will be lower than when using $\hat{\tau}$.

4 Oracle Designs

Our goal is to design a treatment allocation approach that minimizes the risk given a particular estimator. We begin by analyzing the non-adaptive setting, focusing only on experimental designs with a fixed total sample size, N . Moreover, we suppose that the potential outcome variances V_0, \dots, V_K are known *a priori*. These are “oracle” designs, insofar as the V_k are essentially never known in practice and must be estimated directly from the data. However, this setting allows us to gain intuition into the behavior of risk-minimizing designs when using the estimators $\hat{\tau}, \hat{\delta}_B, \hat{\delta}_S$ and $\hat{\delta}_D$.

4.1 A Modified Neyman Allocation

In the standard Neyman Allocation approach, treatment allocation is in proportion to the arm standard deviations $\sqrt{V_k}$. This approach minimizes the expected squared error when estimating the mean for each arm. However, our goal is slightly different; we want to minimize the variance of estimating each *treatment effect*.

Suppose we use the difference-in-means estimator $\hat{\tau} = (\hat{\tau}_1, \dots, \hat{\tau}_K)$ to estimate τ . In this case, the risk of our estimator is

$$\mathcal{R}(\hat{\tau}, \tau) = \text{tr}(\Sigma) = \sum_{k=1}^K \frac{V_0}{n_0} + \frac{V_k}{n_k} = \frac{KV_0}{n_0} + \sum_{k=1}^K \frac{V_k}{n_k}.$$

Hence, obtaining the risk-minimizing allocation of units to treatment arms is equivalent to solving the following optimization problem (Problem 4):

$$\begin{aligned} \min_{n_0, \dots, n_K} \quad & \frac{KV_0}{n_0} + \sum_{k=1}^K \frac{V_k}{n_k} \\ \text{subject to} \quad & \sum_{k=0}^K n_k = N, \\ & 0 < n_0, \dots, n_K. \end{aligned} \tag{4}$$

This is a convex problem whose solution is a slight modification to the standard Neyman Allocation.

Lemma 4. *When using the difference-in-means estimator, the risk-minimizing treatment allocation is*

$$n_0^* = \frac{N\sqrt{KV_0}}{\sqrt{KV_0} + \sum_{\ell=1}^K \sqrt{V_\ell}} \quad \text{and} \quad n_k^* = \frac{N\sqrt{V_k}}{\sqrt{KV_0} + \sum_{\ell=1}^K \sqrt{V_\ell}} \text{ for } k = 1, \dots, K.$$

Proof. See the Appendix, Section D.

4.2 Minimizers in the Low Signal-to-Noise Ratio Regime

The Neyman Allocation provides a useful starting place for choosing a treatment allocation that minimizes the risk using a shrinkage estimator. For any $g(\mathbf{X})$ satisfying the conditions of Lemma 1, the allocation which minimizes the risk of estimator

$$\mathbf{X} - g(\mathbf{X}),$$

is encoded in the following optimization problem (Problem 5):

$$\begin{aligned} \min_{n_0, \dots, n_K} \quad & \frac{KV_0}{n_0} + \sum_{k=1}^K \frac{V_k}{n_k} + \mathbb{E} \left(\|g(\mathbf{X})\|_2^2 - 2 \cdot \text{tr}(\Sigma \mathcal{J}_g(\mathbf{X})) \right) \\ \text{subject to} \quad & \sum_{k=0}^K n_k = N, \\ & 0 < n_0, \dots, n_K. \end{aligned} \tag{5}$$

In this form, we can interpret

$$\Delta = \mathbb{E} \left(\|g(\mathbf{X})\|_2^2 - 2 \cdot \text{tr}(\Sigma \mathcal{J}_g(\mathbf{X})) \right)$$

as a regularization term added to the objective in Problem 4.

Assuming the regularization effect is relatively small, the solutions to Problem 5 will be “local” to the Neyman allocation $\mathbf{n}^* = (n_0^*, \dots, n_K^*)$ and the corresponding λ^* . Hence, we can make headway in characterizing the optimizers of Problem 5 by analyzing the behavior of the objective near the Neyman allocation.

We focus on the regime in which the signal to noise ratio is low. Formally, we assume both that $\boldsymbol{\tau}^T \boldsymbol{\Sigma}_{\text{NA}}^{-1} \boldsymbol{\tau}$ is small and that $\|\boldsymbol{\tau}\|_2^2 \ll \text{tr}(\boldsymbol{\Sigma}_{\text{NA}})$. This assumption restricts to the regime where our shrinkage estimators can yield meaningful performance gains, as is widely discussed in the Empirical Bayes literature (see e.g. Efron, 2012). In less noisy regimes, applying a shrinkage estimator provides less benefit.

4.2.1 Bock’s Estimator

Bock’s estimator $\hat{\boldsymbol{\delta}}_B$ admits the most straightforward analysis. Applying Lemma 1 to Bock’s estimator yields the risk

$$\mathcal{R}(\hat{\boldsymbol{\delta}}_B, \boldsymbol{\tau}) = \text{tr}(\boldsymbol{\Sigma}) + (\tilde{p}^2 - 4)\mathbb{E}\left(\frac{\|\hat{\boldsymbol{\tau}}\|_2^2}{(\hat{\boldsymbol{\tau}}^T \boldsymbol{\Sigma}^{-1} \hat{\boldsymbol{\tau}})^2}\right) - 2(\tilde{p} - 2)\text{tr}(\boldsymbol{\Sigma})\mathbb{E}\left(\frac{1}{\hat{\boldsymbol{\tau}}^T \boldsymbol{\Sigma}^{-1} \hat{\boldsymbol{\tau}}}\right). \quad (6)$$

This expression depends on $\hat{\boldsymbol{\tau}}$ only through the distributions of $\|\hat{\boldsymbol{\tau}}\|_2^2$ and $\hat{\boldsymbol{\tau}}^T \boldsymbol{\Sigma}^{-1} \hat{\boldsymbol{\tau}}$, which exhibit special structure when $\boldsymbol{\tau} = \mathbf{0}$. Hence, our analysis begins with the following result.

Lemma 5. *Suppose $K > 2$. Then*

$$\mathcal{R}(\hat{\boldsymbol{\delta}}_B, \mathbf{0}) = \text{tr}(\boldsymbol{\Sigma}) \left(1 - \frac{2(\tilde{p} - 2)}{K} + \frac{(\tilde{p} - 2)^2}{K(K - 2)}\right). \quad (7)$$

Proof. See the Appendix, Section E.

The risk expression in Equation 7 depends on the allocation of units to treatment arms only through the value of $\tilde{p} = \text{tr}(\boldsymbol{\Sigma})/\lambda_{\max}(\boldsymbol{\Sigma})$. Recall that $0 \leq \tilde{p} \leq K$. Moreover, this risk decreases monotonically as \tilde{p} increases. The following result allows us to characterize the \tilde{p} -maximizing allocation.

Lemma 6. *Suppose that*

$$\left(\max_{k \geq 1} \sqrt{V_k} - \min_{k \geq 1} \sqrt{V_k}\right) \leq \frac{1}{2} \sqrt{KV_0}. \quad (8)$$

Then evaluated at the Neyman allocation $\mathbf{n}^ = (n_0^*, \dots, n_K^*)$,*

$$\frac{\partial \tilde{p}}{\partial n_0} > \max_{k \geq 1} \frac{\partial \tilde{p}}{\partial n_k}.$$

Proof. See the Appendix, Section F.

Lemma 5 tells us that, under $\boldsymbol{\tau} = \mathbf{0}$, the optimizing allocation for Bock’s estimator will be the one that makes \tilde{p} as large as possible. Lemma 6 tells us that, under a mild condition preventing extreme heteroscedasticity across the potential outcome variances, the \tilde{p} -maximizing allocation will assign more units to the control arm than the Neyman allocation.

Next, we extend our reasoning from the case in which $\boldsymbol{\tau} = \mathbf{0}$ to the low signal-to-noise regime. We define the signal-to-noise ratio as

$$\kappa = \boldsymbol{\tau}^T \boldsymbol{\Sigma}^{-1} \boldsymbol{\tau}$$

and suppose $\kappa \leq \epsilon$ for a sufficiently small value of ϵ . A first-order expansion of the risk in Eq. 6 around $\kappa = 0$ yields

$$\mathcal{R}(\hat{\boldsymbol{\delta}}_B, \boldsymbol{\tau}) = \mathcal{R}(\hat{\boldsymbol{\delta}}_B, \mathbf{0}) + \frac{1}{K-2} \left(\frac{2(\tilde{p} - 2)}{K} - \frac{\tilde{p}^2 - 4}{K^2} \right) \text{tr}(\boldsymbol{\Sigma}) \cdot \kappa + \mathcal{O}(\kappa^2). \quad (9)$$

At the Neyman allocation \mathbf{n}^* and under the fixed-budget constraint $\sum_{k=0}^K n_k = N$, the first-order variation of $\text{tr}(\boldsymbol{\Sigma})$ is zero. This means that a Taylor approximation to the function will have zero coefficient on the linear term in any direction that satisfies the constraint. Thus, near the Neyman allocation, the risk expansion in Equation 9 depends on the treatment allocation only through \tilde{p} and $\kappa = \boldsymbol{\tau}^T \boldsymbol{\Sigma}^{-1} \boldsymbol{\tau}$ up to first order. Moreover, the latter dependency is assumed small due to the $\kappa \leq \epsilon$ constraint. Finally, while the second term is increasing in \tilde{p} , this dependency is similarly small due to the multiplicative dependency on small κ .

Equation 9 shows that, locally to the Neyman Allocation and in the low signal-to-noise regime, $\mathcal{R}(\hat{\delta}_B, \tau)$ is a small perturbation of $\mathcal{R}(\hat{\delta}_B, \mathbf{0})$. Thus, for sufficiently small κ , the risk-minimizing allocation for $\mathcal{R}(\hat{\delta}_B, \tau)$ is close to a \tilde{p} -maximizing allocation at $\tau = \mathbf{0}$. Hence, in the relevant setting, we have shown that the minimizer of Bock's estimator will tend to assign more units to the control arm than the Neyman allocation.

4.2.2 SURE-Min Estimator

The SURE-minimizing estimator $\hat{\delta}_S$ does not admit a closed-form risk expression when $\tau = 0$. Hence, we rely on a sequence of approximations to characterize the behavior of risk-minimizing allocations.

Applying Lemma 1 yields

$$\mathcal{R}(\hat{\delta}_S, \tau) = \text{tr}(\Sigma) + 4\text{tr}(\Sigma)\mathbb{E}\left(\frac{\hat{\tau}^\top \Sigma \hat{\tau}}{\|\hat{\tau}\|_2^4}\right) - \text{tr}(\Sigma)^2 \mathbb{E}\left(\frac{1}{\|\hat{\tau}\|_2^2}\right). \quad (10)$$

The expectations are not analytically tractable. To obtain a usable approximation, we approximate the Gaussian quadratic forms appearing in Equation 10 using the moment-matching approach of Sattherthwaite (1946). Namely, we approximate

$$\|\hat{\tau}\|_2^2 \sim \text{Gamma}\left(\frac{m^2}{v}, \frac{v}{m}\right),$$

where

$$m := \mathbb{E}(\|\hat{\tau}\|_2^2) = \text{tr}(\Sigma) + \|\tau\|_2^2, \quad v := \text{var}(\|\hat{\tau}\|_2^2) = 2\text{tr}(\Sigma^2) + 4\tau^\top \Sigma \tau.$$

Via this approximation, we obtain a tractable expression for the reciprocal expectation appearing in Equation 10:

$$\mathbb{E}\left(\frac{1}{\|\hat{\tau}\|_2^2}\right) \approx \frac{\text{tr}(\Sigma) + \|\tau\|_2^2}{(\text{tr}(\Sigma) + \|\tau\|_2^2)^2 - 2\text{tr}(\Sigma^2) - 4\tau^\top \Sigma \tau}.$$

To approximate the ratio expectation, we employ the crude approximation

$$\hat{\tau}^\top \Sigma \hat{\tau} \approx \frac{\mathbb{E}(\hat{\tau}^\top \Sigma \hat{\tau})}{\mathbb{E}(\|\hat{\tau}\|_2^2)} \|\hat{\tau}\|_2^2,$$

which holds exactly when Σ is proportional to the identity. Using

$$\mathbb{E}(\hat{\tau}^\top \Sigma \hat{\tau}) = \text{tr}(\Sigma^2) + \tau^\top \Sigma \tau,$$

this yields the approximation

$$\mathbb{E}\left(\frac{\hat{\tau}^\top \Sigma \hat{\tau}}{\|\hat{\tau}\|_2^4}\right) \approx \frac{\text{tr}(\Sigma^2) + \tau^\top \Sigma \tau}{\text{tr}(\Sigma) + \|\tau\|_2^2} \mathbb{E}\left(\frac{1}{\|\hat{\tau}\|_2^2}\right).$$

Substituting these approximations into Equation 10 yields a closed-form approximation to the risk. In the low signal-to-noise regime, we treat $\|\tau\|_2^2$ and $\tau^\top \Sigma \tau$ as small relative to $\text{tr}(\Sigma)$ and $\text{tr}(\Sigma^2)$, and retain only the leading terms obtained by setting $\tau = \mathbf{0}$ inside the approximations. This yields

$$\mathcal{R}(\hat{\delta}_S, \tau) \approx \text{tr}(\Sigma) \left(1 + \frac{4\text{tr}(\Sigma^2) - \text{tr}(\Sigma)^2}{\text{tr}(\Sigma)^2 - 2\text{tr}(\Sigma^2)}\right). \quad (11)$$

We recall that the risk of the difference-in-means estimator is simply $\text{tr}(\Sigma)$, so the Neyman allocation \mathbf{n}^* minimizes $\text{tr}(\Sigma)$ subject to the sample size constraint $\sum_{k=0}^K n_k = N$. As a result, small reallocations of units to arms around \mathbf{n}^* that respect this constraint leave the value of $\text{tr}(\Sigma)$ essentially unchanged. However, such reallocations generally alter the value of $\text{tr}(\Sigma^2)$. Moreover, for a given value of $\text{tr}(\Sigma)$, the approximate risk in Equation (11) increases with $\text{tr}(\Sigma^2)$. Hence, near the Neyman allocation, the SURE-minimizing allocation can be viewed as one that preserves $\text{tr}(\Sigma)$ while making $\text{tr}(\Sigma^2)$ as small as possible.

We use the derivative to characterize the most efficient means of decreasing $\text{tr}(\Sigma^2)$. Because

$$\text{tr}(\Sigma^2) = K^2 \frac{V_0^2}{n_0^2} + 2 \frac{V_0}{n_0} \sum_{k=1}^K \frac{V_k}{n_k} + \sum_{k=1}^K \frac{V_k^2}{n_k^2},$$

we see that

$$\frac{\partial \text{tr}(\Sigma^2)}{\partial n_0} = -\frac{2V_0}{n_0^2} \left(K^2 \frac{V_0}{n_0} + \sum_{k=1}^K \frac{V_k}{n_k} \right) \quad \text{and} \quad \frac{\partial \text{tr}(\Sigma^2)}{\partial n_k} = -\frac{2V_k}{n_k^2} \left(\frac{V_0}{n_0} + \frac{V_k}{n_k} \right), \quad k = 1, \dots, K.$$

Evaluated at the Neyman allocation, these are

$$\frac{\partial \text{tr}(\Sigma^2)}{\partial n_0} = -2S_{\text{NA}}^3 \left(\sqrt{KV_0} + \frac{1}{K} \sum_{k=1}^K \sqrt{V_k} \right) \quad \text{and} \quad \frac{\partial \text{tr}(\Sigma^2)}{\partial n_k} = -2S_{\text{NA}}^3 \left(\sqrt{\frac{V_0}{K}} + \sqrt{V_k} \right). \quad (12)$$

The expressions in (12) allow us to quantify which arms will be allocated more units. Unless V_0 is extremely small relative to the other V_k values, the derivative with respect to n_0 will be much larger in magnitude than the other derivatives. Hence, the $\mathcal{R}(\hat{\delta}_S, \tau)$ -minimizing allocation optimizer will again shift units toward the control arm relative to the Neyman Allocation; this strategy is the most efficient way to decrease $\text{tr}(\Sigma^2)$ while leaving $\text{tr}(\Sigma)$ essentially unchanged. Moreover, among the active treatments, we observe that $\partial \text{tr}(\Sigma^2)/\partial n_k$ is more negative when V_k is larger. Hence, the SURE-Min risk minimizer will also tend to reallocate units toward the treatment arms with the largest potential outcome variances.

4.2.3 Dimmery's Estimator

Lastly, Dammery's estimator $\hat{\delta}_D$ also only admits a heuristic analysis, and we again focus on the low signal-to-noise regime. Using Lemma 1, its risk can be written as

$$\mathcal{R}(\hat{\delta}_D, \tau) = \text{tr}(\Sigma) + \mathbb{E} \left(\frac{(K-2)^2}{\|\hat{\tau}\|_2^4} \hat{\tau}^\top \Sigma_{\star}^2 \hat{\tau} + \frac{4(K-2)}{\|\hat{\tau}\|_2^4} \hat{\tau}^\top \Sigma \Sigma_{\star} \hat{\tau} - \frac{2(K-2)\text{tr}(\Sigma_{\star}^2)}{\|\hat{\tau}\|_2^2} \right), \quad (13)$$

where Σ_{\star} is the diagonal matrix whose diagonal entries are equal to the diagonal entries of Σ .

To estimate this quantity, we assume the signal-to-noise ratio is small such that τ is small and $\hat{\tau}$ behaves approximately as $\mathcal{N}(\mathbf{0}, \Sigma)$. We employ the same two crude approximations from the prior section, namely

$$\mathbb{E} \left(\frac{1}{\|\hat{\tau}\|_2^2} \right) \approx \frac{1}{\text{tr}(\Sigma)}, \quad \text{and} \quad \mathbb{E} \left(\frac{\hat{\tau}^\top A \hat{\tau}}{\|\hat{\tau}\|_2^4} \right) \approx \frac{\mathbb{E}(\hat{\tau}^\top A \hat{\tau})}{\text{tr}(\Sigma)^2} = \frac{\text{tr}(A\Sigma)}{\text{tr}(\Sigma)^2},$$

where A is any symmetric matrix. Applying these approximations to Equation 13 gives the proxy value

$$\mathcal{R}(\hat{\delta}_D, \tau) \approx \text{tr}(\Sigma) + \frac{(K-2)^2 \text{tr}(\Sigma_{\star}^2 \Sigma) + 4(K-2) \text{tr}(\Sigma \Sigma_{\star} \Sigma)}{\text{tr}(\Sigma)^2} - \frac{2(K-2) \text{tr}(\Sigma_{\star}^2)}{\text{tr}(\Sigma)}. \quad (14)$$

To make Expression 14 more explicit, recall that each diagonal entry of Σ and Σ_{\star} is equal to $V_k/n_k + V_0/n_0$. Hence,

$$\begin{aligned} \text{tr}(\Sigma_{\star}^2) &= \sum_{k=1}^K \left(\frac{V_k}{n_k} + \frac{V_0}{n_0} \right)^2, \quad \text{tr}(\Sigma_{\star}^2 \Sigma) = \sum_{k=1}^K \left(\frac{V_k}{n_k} + \frac{V_0}{n_0} \right)^3, \quad \text{and} \\ \text{tr}(\Sigma \Sigma_{\star} \Sigma) &= \sum_{k=1}^K \left(\frac{V_k}{n_k} + \frac{V_0}{n_0} \right)^3 + (K-1) \left(\frac{V_0}{n_0} \right)^2 \sum_{k=1}^K \left(\frac{V_k}{n_k} + \frac{V_0}{n_0} \right). \end{aligned}$$

Again, we recall that the Neyman allocation \mathbf{n}^* minimizes $\text{tr}(\Sigma)$ subject to $\sum_{k=0}^K n_k = N$. As for the SURE-Min estimator, small reallocations around \mathbf{n}^* that respect the sample size constraint leave $\text{tr}(\Sigma)$ essentially unchanged, but can change $\text{tr}(\Sigma_{\star}^2)$, $\text{tr}(\Sigma_{\star}^2 \Sigma)$, and $\text{tr}(\Sigma \Sigma_{\star} \Sigma)$. Holding $\text{tr}(\Sigma)$ fixed, Expression 14 decreases with $\text{tr}(\Sigma_{\star}^2)$ and increases with $\text{tr}(\Sigma_{\star}^2 \Sigma)$ and $\text{tr}(\Sigma \Sigma_{\star} \Sigma)$.

Intuitively, we observe that increasing n_0 reduces every such diagonal entry simultaneously. Thus, increasing the size of the control arm has the effect of most rapidly decreasing the cubic contributions of $\sum_{k=1}^K \left(\frac{V_k}{n_k} + \frac{V_0}{n_0} \right)^3$ within both $\text{tr}(\Sigma_{\star}^2 \Sigma)$ and $\text{tr}(\Sigma \Sigma_{\star} \Sigma)$, while increasing the quadratic quantities in $\text{tr}(\Sigma_{\star}^2)$ more slowly and leaving $\text{tr}(\Sigma)$ nearly unchanged. Likewise, among active treatment arms, shifting units from a low-variance arm to a high-variance arm (i.e. increasing n_k when V_k is large and decreasing n_j when V_j is small, under the sample size constraint) tends to equalize the $\frac{V_k}{n_k}$ terms. This shift reduces the variability across the $\left(\frac{V_k}{n_k} + \frac{V_0}{n_0} \right)$ values and thus again most directly lowers the aggregate cubic contributions.

Thus, a heuristic analysis points toward similar behavior among the minimizers of $\hat{\delta}_S$ and $\hat{\delta}_D$. Relative to Neyman, both minimizing allocations will tend to increase n_0 and shift more units toward treatment arms with larger values of V_k . In contrast, the minimizer of Bock's estimator $\hat{\delta}_B$ will increase n_0 , but will not prioritize high-variance arms.

4.3 Simulated Static Allocations

To complement our heuristic analysis, we conduct simulations in simple regimes where the potential outcome variances $\mathbf{V} = (V_0, \dots, V_K)$ are known. For each setting, we compute the non-adaptive Neyman allocation \mathbf{n}^* and compare it to the allocations that minimize the risk of each shrinkage estimator. This strategy allows us to empirically assess how minimizing the risks of $\hat{\delta}_B, \hat{\delta}_S, \hat{\delta}_D$ perturb the baseline Neyman allocation.

4.3.1 Computing Risk-Minimizing Allocations

Denote as $\mathcal{R}_{\hat{\delta}}(\mathbf{n}, \mathbf{V}, \boldsymbol{\tau})$ the risk of estimator $\hat{\delta}$ evaluated at allocation \mathbf{n} under potential outcome variances \mathbf{V} and true treatment effects $\boldsymbol{\tau}$. Notably, $\mathcal{R}_{\hat{\delta}}(\mathbf{n}, \mathbf{V}, \boldsymbol{\tau})$ is *not* a convex function of the allocations n_0, \dots, n_K for any of our shrinkage estimators. Hence, practically, we achieve the risk minimizations through a greedy swapping algorithm. Define

$$\mathbf{n}^{(j)} = \{n_0^{(j)}, \dots, n_K^{(j)}\} \in \mathbb{Z}^{K+1}$$

as the allocation of units to treatment arms at iteration j of the algorithm. Next, define the set of potential swaps

$$D^{(j)} = \{\mathbf{n} \in \mathbb{Z}^{K+1} \mid \mathbf{n} \text{ swaps exactly one unit across treatment arms from } \mathbf{n}^{(j)}\}.$$

Because there are $K+1$ treatment arms, the “swap set” $D^{(j)}$ will contain $K(K+1)$ possible allocations. At each iteration of the algorithm, we simply move in the direction of the swap that most reduces the risk. This approach is encoded below, in Algorithm 15:

```

Start with the Neyman allocation  $\mathbf{n}^{(0)} = \mathbf{n}^*$ .
For iteration  $j = 1, 2, \dots$ :
  For each potential allocation  $\mathbf{n} \in D^{(j-1)}$ :
    Compute  $\mathcal{R}_{\hat{\delta}}(\mathbf{n}, \mathbf{V}, \boldsymbol{\tau})$ .
    Set  $\mathbf{n}^{(j)} = \arg \min_{\mathbf{n} \in D^{(j-1)}} \mathcal{R}_{\hat{\delta}}(\mathbf{n}, \mathbf{V}, \boldsymbol{\tau})$  (15)
    If  $\mathcal{R}_{\hat{\delta}}(\mathbf{n}^{(j)}, \mathbf{V}, \boldsymbol{\tau}) \geq \mathcal{R}_{\hat{\delta}}(\mathbf{n}^{(j-1)}, \mathbf{V}, \boldsymbol{\tau})$ 
      Return  $\mathbf{n}^{(j-1)}$ .

```

For details on how $\mathcal{R}_{\hat{\delta}}(\mathbf{n}, \mathbf{V}, \boldsymbol{\tau})$ is computed, see Section 5.1. Additionally, while Algorithm 15 could plausibly get stuck at local minima, we find in practice that the algorithm’s output tends to be unchanged regardless of the starting point.

4.3.2 Simulation Setup

We simulate data given a variety of data-generating regimes. Throughout, we fix the total sample size at $N = 1,000$ and compute, for each setting, the Neyman allocation \mathbf{n}^* as well as the allocations that minimize the risks of $\hat{\delta}_B, \hat{\delta}_S$, and $\hat{\delta}_D$ using the greedy swapping approach (Algorithm 15).

We alter four key features across our simulations: the number of treatment arms K ; the magnitude of the control potential outcome variance V_0 relative to the active treatment-arm variances $\{V_k\}_{k=1}^K$; the sparsity of $\boldsymbol{\tau}$; and the signal-to-noise ratio $\kappa = \boldsymbol{\tau}^\top \boldsymbol{\Sigma}_{\text{NA}}^{-1} \boldsymbol{\tau}$.

To sample the potential outcome variances, we first sample V_k for the active treatment arms $k = 1, \dots, K$ are drawn *i.i.d.* from a log normal distribution with log-location parameter of $\log(350)$ and log-standard-deviation parameter 0.60. These values are then sorted such that $V_1 = V_{(1)}, \dots, V_K = V_{(K)}$; this sorting will later help us to reason about reallocations across active treatment arms according to their relative variances. Next, we consider two control-variance regimes. In the low-control-variance regime, V_0 is equal to half of the average treatment arm potential outcome variance, i.e. $V_0 = \frac{1}{2} \cdot K^{-1} \sum_{k=1}^K V_k$. In the high control-variance regime, V_0 is equal to four times the average treatment arm variance, i.e. $V_0 = 4 \cdot K^{-1} \sum_{k=1}^K V_k$.

The treatment effects $\boldsymbol{\tau}$ are sampled to ensure the desired sparsity and signal-to-noise-ratio. First, we consider two configurations for the parsimony of the “signal” $\boldsymbol{\tau}$. In the dense setting, an unscaled $\tilde{\boldsymbol{\tau}}$ is sampled from a $\text{Unif}([1, 2])$ distribution, resulting in all causal effects having comparable magnitude.

In the sparse setting, $\tilde{\boldsymbol{\tau}} = (1, \dots, 0)$ has only a single nonzero entry, which corresponds to the first arm (and thus, due to the sorting, also corresponding to the smallest potential outcome variance among the active treatment arms).

Once the unscaled effects are sampled, they are scaled to give $\boldsymbol{\tau}$ that meets the desired signal-to-noise-ratio $\kappa = \boldsymbol{\tau}^\top \boldsymbol{\Sigma}_{\mathbf{NA}}^{-1} \boldsymbol{\tau}$. We recall that $\boldsymbol{\Sigma}_{\mathbf{NA}}$ is the covariance matrix at the Neyman allocation. Hence, κ is an approximation to the signal-to-noise ratio at the true minimizer, as the covariance matrix itself changes as we reallocate units across treatment arms.

Tables 1 and 2 report the results of all the simulations, across the grid of regimes:

$$K \in \{6, 12\}, \quad V_0 \in \{\text{low, high}\}, \quad \boldsymbol{\tau} \in \{\text{dense, sparse}\}, \quad \kappa \in \{0, 3, 9\}.$$

Note that when $\kappa = 0$, we must have $\boldsymbol{\tau} = \mathbf{0}$, so $\boldsymbol{\tau}$ is neither dense nor sparse. This setting is reflected in the tables with a “–” symbol in the “ $\boldsymbol{\tau}$ shape” column.

4.3.3 Simulation Results

In the simulation results, we compare how the different risk-minimization allocations differ in the relative sizes of different treatment arms, compared to the Neyman allocation. These simulations do not evaluate the performance of any of the risk-minimization allocations, because the oracle setting is not a realistic setting for evaluating performance. Section 5 contains simulations that evaluate performance in an adaptive setting.

Large reallocations to the control arm, attenuated by signal strength. Table 1 shows the share of units allocated to the control arm across all settings and designs. The allocations reflect the most stable pattern in our simulations: all shrinkage-risk-minimizing designs allocate more units to control than the Neyman Allocation, with the magnitude of this reallocation mediated by signal strength, dimension, and the sparsity of the treatment effects. Reallocation toward control are largest with no signal, $\kappa = 0$; attenuate modestly with moderate signal, $\kappa = 3$; and are typically small with large signal, $\kappa = 9$. Moreover, reallocations toward control are typically larger when there are more arms, $K = 12$ compared to $K = 6$. These patterns are consistent across both control-variance regimes.

Table 1 also reveals that the distinction between sparse and dense treatment effects plays an important role in determining the magnitude of control reallocations, particularly for Bock’s estimator $\hat{\boldsymbol{\delta}}_B$. When $\kappa > 0$, reallocations toward control under $\hat{\boldsymbol{\delta}}_B$ are substantially larger when $\boldsymbol{\tau}$ is sparse than when it is dense, often by a wide margin. In several settings, sparse signals lead to control reallocations for Bock that are comparable to, or even exceed, those observed at $\kappa = 0$, whereas dense signals produce markedly more moderate shifts.

This pattern mirrors our heuristic investigation, which showed that the risk-minimizing allocations for all estimators favor more control units relative to the Neyman allocation \mathbf{n}^* . However, the behavior is not uniform across estimators. Generally, the minimizing assignment for Bock’s estimator $\hat{\boldsymbol{\delta}}_B$ exhibits the largest reallocation toward control, followed by the SURE-min estimator $\hat{\boldsymbol{\delta}}_S$ and then Dimmery’s estimator $\hat{\boldsymbol{\delta}}_D$. For the SURE-min and Dimmery estimators, the sparse vs. dense distinction is considerably less pronounced: reallocations toward control are modestly larger under sparse signals, but the key driver of control reallocation for these estimators is simply the overall signal-to-noise ratio.

An exception to the ordering of control reallocation across the shrinkage estimators is visible only in the high- V_0 regime, with nonzero κ and dense $\boldsymbol{\tau}$. In these simulations, reallocations toward control are typically larger for the SURE-min estimator than for Bock’s estimator. Otherwise, Bock’s estimator exhibits the strongest and most persistent preference for allocating additional units to the control arm.

Reallocation across active treatment arms. Beyond reallocations toward the control arm, the risk-minimizing designs also differ in how they redistribute samples across the active treatment arms. Table 2 reports reallocations toward treatment arm 1 and toward treatment arm K , measured relative to the Neyman allocation. Recall that treatment arm 1 has the smallest potential outcome variance among the active treatments, and the sole nonzero signal when $\boldsymbol{\tau}$ is sparse. Treatment arm K has the largest potential outcome variance among the active treatments.

In the case of Bock’s estimator, the allocation to active treatment arms does not vary substantially across regimes. The minimizing allocations for Bock’s estimator never increase the share of units assigned to the first active treatment arm, and frequently reduce this share. The same behavior is evident for the K^{th} treatment arm. The behavior is essentially insensitive to the dimension, control arm variance, sparsity of $\boldsymbol{\tau}$, and signal to noise ratio κ . This pattern reflects the central tendency of the minimization

for Bock's estimator, which focuses almost exclusively on reallocating units to the control arm in order to reduce the shrinker risk.

The minimizing allocations for the SURE-min estimator are more variable. The risk minimizer allocates units away from treatment arm 1 when the signal-to-noise ratio is small, but tends to allocate units toward the arm when κ grows, especially when the signal is sparse. Meanwhile, units are never allocated toward the K^{th} treatment arm, and are typically allocated away from it.

Dimmery's estimator exhibits the most variable behavior across simulation conditions. When the signal-to-noise ratio is zero or when the signal is dense, the minimizer either allocates fewer units to the first treatment arm, or just a few more units. However, in the case of a sparse signal, Dimmery's estimator allocates many more units to the first treatment arm, exhibiting a strong preference for "overweighting" the arm with a strong signal, even though that arm exhibits low potential outcome variances. These allocations also uniformly allocate units away from the K^{th} treatment arm, doing so most dramatically in the sparse- τ regime.

Table 1: Risk-minimizing allocations for $N = 1,000$: control share.

K	V_0	regime	τ	shape	κ	Neyman n_0^*/N	Bock $\Delta n_0/N$	SURE-min $\Delta n_0/N$	Dimmery $\Delta n_0/N$
6	high	—	0	0.40		+0.22		+0.14	+0.11
6	high	dense	3	0.39		+0.09		+0.10	+0.07
6	high	sparse	3	0.40		+0.16		+0.09	+0.08
6	high	dense	9	0.40		+0.03		+0.07	+0.05
6	high	sparse	9	0.39		+0.08		+0.04	+0.07
6	low	—	0	0.22		+0.23		+0.07	+0.05
6	low	dense	3	0.23		+0.09		+0.07	+0.05
6	low	sparse	3	0.18		+0.16		+0.03	+0.03
6	low	dense	9	0.22		+0.03		+0.05	+0.04
6	low	sparse	9	0.19		+0.10		+0.02	+0.04
12	high	—	0	0.31		+0.34		+0.15	+0.13
12	high	dense	3	0.32		+0.11		+0.12	+0.10
12	high	sparse	3	0.30		+0.32		+0.14	+0.12
12	high	dense	9	0.30		+0.05		+0.08	+0.07
12	high	sparse	9	0.33		+0.18		+0.12	+0.14
12	low	—	0	0.16		+0.35		+0.08	+0.07
12	low	dense	3	0.15		+0.17		+0.07	+0.05
12	low	sparse	3	0.17		+0.33		+0.06	+0.06
12	low	dense	9	0.15		+0.06		+0.06	+0.05
12	low	sparse	9	0.15		+0.26		+0.04	+0.07

Δn_0 represents the change in the proportion of units allocated to the control arm relative to the Neyman allocation n_0^* .

Figures 1, 2, and 3 provide three representative visual summaries of risk-minimizing allocations when $K = 12$. Figure 1 demonstrates the tendency of all shrinker-risk-minimizers – especially Bock's estimator $\hat{\delta}_B$ – to reallocate sample toward the control arm. Figure 2 shows how this pattern attenuates at larger values of the signal-to-noise ratio, especially for $\hat{\delta}_S$ and $\hat{\delta}_D$. Figure 3 reflects how, other things equal, the $\hat{\delta}_D$ -minimizing allocation tends to assign units to the arm with strong signal when τ is sparse.

5 Adaptive Risk Minimization

The approach in Section 4 allows us to characterize the risk-minimizing designs, but it does not provide a pathway to sequential adaptivity because the parameters are assumed known in the design phase. In this section, we introduce a simple algorithm for an adaptive experiment that seeks to minimize the risk of $\hat{\delta}_B$, $\hat{\delta}_S$, or $\hat{\delta}_D$.

Table 2: Risk-minimizing allocations for $N = 1,000$: reallocations toward treatment arm 1 and treatment arm K .

K	V_0	regime	τ shape	κ	$\Delta n_1/N$			$\Delta n_K/N$		
					Bock	SURE-min	Dimmery	Bock	SURE-min	Dimmery
6	high	—	0	0	-0.03	-0.03	-0.03	-0.04	-0.02	-0.01
6	high	dense	3	-0.01	-0.01	+0.02	-0.02	-0.02	-0.02	-0.02
6	high	sparse	3	-0.03	+0.02	+0.07	-0.03	-0.02	-0.03	-0.03
6	high	dense	9	+0.00	+0.00	+0.01	-0.01	-0.02	-0.03	-0.03
6	high	sparse	9	-0.02	+0.04	+0.10	-0.01	-0.02	-0.06	-0.06
6	low	—	0	-0.04	-0.02	-0.03	-0.03	-0.01	-0.01	-0.01
6	low	dense	3	-0.02	-0.01	+0.02	+0.00	+0.00	-0.01	-0.01
6	low	sparse	3	-0.05	+0.03	+0.12	-0.02	-0.01	-0.08	-0.08
6	low	dense	9	-0.01	-0.01	+0.00	-0.01	-0.01	-0.01	-0.01
6	low	sparse	9	-0.04	+0.05	+0.13	-0.01	-0.01	-0.10	-0.10
12	high	—	0	-0.02	-0.02	-0.02	-0.02	-0.01	-0.01	-0.01
12	high	dense	3	-0.01	-0.01	+0.00	+0.00	-0.01	-0.01	-0.01
12	high	sparse	3	-0.03	+0.00	+0.06	+0.00	-0.01	-0.05	-0.05
12	high	dense	9	+0.00	+0.00	+0.01	-0.01	-0.01	-0.01	-0.01
12	high	sparse	9	-0.02	+0.01	+0.07	+0.00	-0.01	-0.06	-0.06
12	low	—	0	-0.02	-0.01	-0.02	-0.01	+0.00	+0.00	+0.00
12	low	dense	3	-0.01	-0.01	-0.02	-0.01	+0.00	+0.00	+0.00
12	low	sparse	3	-0.03	+0.00	+0.08	+0.01	+0.00	-0.06	-0.06
12	low	dense	9	-0.01	-0.01	-0.01	-0.01	-0.01	-0.01	-0.01
12	low	sparse	9	-0.02	+0.02	+0.09	+0.00	-0.01	-0.07	-0.07

Δn_1 and Δn_K denote the change in the proportion of units allocated to treatment arms 1 and K , respectively, relative to the Neyman allocation values n_1^* and n_K^* . Positive values indicate reallocations toward the corresponding arm.

5.1 Efficient Risk Computation

For each of our candidate estimators, we can use Equation 1 to obtain the risk. In each case, the resultant expression is a linear combination of ratios of Gaussian quadratic forms.

We use $\hat{\delta}_B$ as our motivating example. As discussed in Section 4

$$\begin{aligned} \mathcal{R}(\hat{\delta}_B, \tau) &= \text{tr}(\Sigma) + \mathbb{E} \left(\frac{(\tilde{p} - 2)^2 \|\hat{\tau}\|_2^2}{(\hat{\tau}^\top \Sigma^{-1} \hat{\tau})^2} - \frac{2(\tilde{p} - 2)}{\hat{\tau}^\top \Sigma^{-1} \hat{\tau}} \text{tr}(\Sigma) + \frac{4(\tilde{p} - 2) \|\hat{\tau}\|_2^2}{(\hat{\tau}^\top \Sigma^{-1} \hat{\tau})^2} \right) \\ &= \text{tr}(\Sigma) + (\tilde{p}^2 - 4) \mathbb{E} \left(\frac{\|\hat{\tau}\|_2^2}{(\hat{\tau}^\top \Sigma^{-1} \hat{\tau})^2} \right) - 2(\tilde{p} - 2) \text{tr}(\Sigma) \mathbb{E} \left(\frac{1}{\hat{\tau}^\top \Sigma^{-1} \hat{\tau}} \right). \end{aligned} \quad (16)$$

Recall that $\hat{\tau}$ is approximately normally distributed. Hence, the two quantities whose expectations we need are ratios of Gaussian quadratic forms. Results from Bao and Kan (2013) provide a simple procedure to turn these expectations into numerical integrals, which can be computed efficiently.

Observe that we can rewrite the risk as

$$\mathcal{R}(\hat{\delta}_B, \tau) = \text{tr}(\Sigma) + (\tilde{p}^2 - 4) \mathbb{E} \left(\frac{\boldsymbol{\theta}^\top \Sigma \boldsymbol{\theta}}{(\boldsymbol{\theta}^\top \boldsymbol{\theta})^2} \right) - 2(\tilde{p} - 2) \text{tr}(\Sigma) \mathbb{E} \left(\frac{1}{(\boldsymbol{\theta}^\top \boldsymbol{\theta})} \right)$$

where $\boldsymbol{\theta} = \Sigma^{-1/2} \hat{\tau} \sim \mathcal{N}(\Sigma^{-1/2} \tau, \mathbf{I}_K)$. All we've done is re-express the expectations in terms of a standard multivariate random variable, which is helpful for applying the Bao and Kan (2013) results.

A direct application of the results in Bao and Kan (2013) yields the following integral expressions:

$$\begin{aligned} \mathbb{E} \left(\frac{\boldsymbol{\theta}^\top \Sigma \boldsymbol{\theta}}{(\boldsymbol{\theta}^\top \boldsymbol{\theta})^2} \right) &= \int_0^\infty (1 + 2t)^{-K/2} \cdot \exp \left(-(\tau^\top \Sigma^{-1} \tau) \cdot \frac{t}{1 + 2t} \right) \cdot \left(\frac{\text{tr}(\Sigma)}{1 + 2t} + \frac{\tau^\top \tau}{(1 + 2t)^2} \right) t \, dt, \text{ and} \\ \mathbb{E} \left(\frac{1}{\boldsymbol{\theta}^\top \boldsymbol{\theta}} \right) &= \int_0^\infty (1 + 2t)^{-K/2} \cdot \exp \left(-(\tau^\top \Sigma^{-1} \tau) \cdot \frac{t}{1 + 2t} \right) dt. \end{aligned} \quad (17)$$

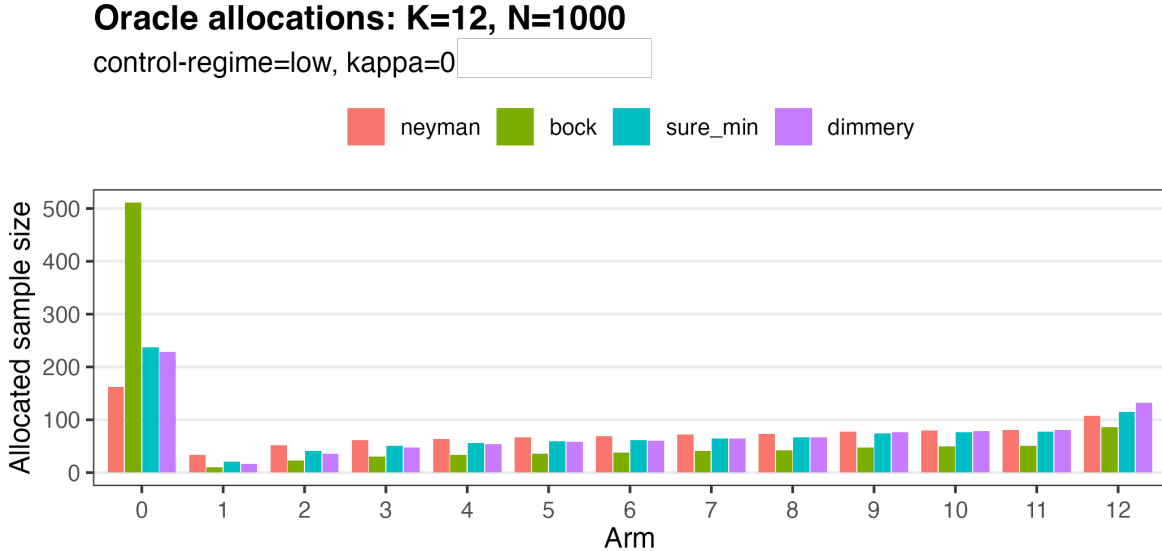


Figure 1: Oracle allocations for $K = 12$ and $N = 1,000$ with low control variance, and $\kappa = 0$. All shrinker-risk-minimizing designs shift mass toward the control arm relative to the Neyman allocation, with the largest control shift under Bock’s estimator $\hat{\delta}_B$. SURE-min $\hat{\delta}_S$ and Dimmery $\hat{\delta}_D$ exhibit the same trend but with smaller magnitude.

Crucially, the integrals in (17) are univariate, and hence can be efficiently computed to high precision. Leveraging a C++ integration into R via RCPP (Eddelbuettel and François, 2011) yields further speed improvements. In Table 3, we provide speed benchmarks in milliseconds over 1,000 repetitions for the computation of the risk of each estimator. The implementations are via RCPP, computed for different values of the problem dimension K . No effort was made to optimize the code, and further improvements at high dimension are likely possible. All benchmarks were run on a 14-inch MacBook Pro with an Apple M4 Pro processor and 24 GB of memory, running MacOS.

Table 3: Avg. computation time (milliseconds) over 1,000 iterations.

Dimension K	Bock ($\hat{\delta}_B$)	SURE-min ($\hat{\delta}_S$)	Dimmery ($\hat{\delta}_D$)
4	0.0049	0.0349	0.0826
6	0.0062	0.1888	0.4608
8	0.0074	0.4956	1.1753
12	0.0117	1.0190	2.4784
16	0.0168	2.4161	5.9049

5.2 Greedy Algorithm

In the adaptive design literature, there are many proposals for the cadence at which treatment assignment rules are updated. Many approaches consider a “pilot” or “warm-up” phase in which treatment assignments are non-adaptive and equal across arms, with the information collected in this phase used to determine a single assignment rule for the latter experimental phase (Blackwell et al., 2022; Cai and Rafi, 2024; Tabord-Meehan, 2018; Hahn et al., 2011). Alternatively, treatment assignment rules may be updated in batches (Li and Owen, 2024; Zhang et al., 2020) or recomputed sequentially with each new arrival (Kato et al., 2020; Dai et al., 2023).

We propose a simple, greedy algorithm that combines several of these approaches. Suppose the adaptive experiment is pre-specified to involve N total units. For the first $N_{\text{burn-in}} \ll N$ arrivals, we assign the treatment according to complete randomization, with equal probability of receiving the control

Oracle allocations: K=12, N=1000

control-regime=low, kappa=9, shape=dense

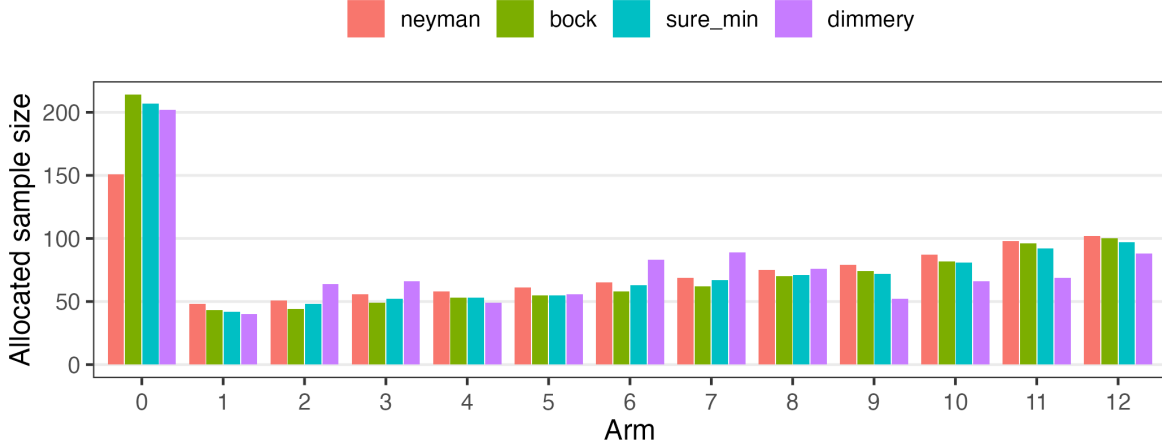


Figure 2: Oracle allocations for $K = 12$ and $N = 1,000$ with low control variance, $\kappa = 9$, and dense $\boldsymbol{\tau}$. Compared to the $\kappa = 0$ case (Figure 1), the shrinkage-driven preference for allocating additional units to control is substantially reduced for all estimators, especially the Bock estimator (though it still favors the control arm most among the three shrinkers).

or any of the K active treatments. Denote as $\hat{\boldsymbol{\tau}}^{(i)}$ the causal estimates after arrival i (computed using the difference-in-mean estimator), and $\hat{\mathbf{V}}^{(i)}$ the estimated potential outcome variances after arrival i (computed using the standard sample variance formula). Moreover, let

$$\mathbf{n}^{(i)} = \left(n_0^{(i)}, \dots, n_K^{(i)} \right)^T \in \mathbb{R}^{K+1}$$

represent the total number of units assigned to each arm after arrival i , and let $\mathbf{e}_k \in \mathbb{R}^{K+1}$ be the vector whose $(k+1)^{\text{th}}$ entry is 1 and whose other entries are 0. For i such that $N_{\text{burn-in}} < i \leq N$, we assign treatment according to the deterministic rule:

$$W_i = \arg \min_{k \in \{0, \dots, K\}} \mathcal{R}_{\hat{\delta}} \left(\mathbf{n}^{(i-1)} + \mathbf{e}_k, \hat{\mathbf{V}}^{(i-1)}, \hat{\boldsymbol{\tau}}^{(i-1)} \right).$$

In words: after the completion of the burn-in period, we assign units to arms based on which assignment will minimize our current estimate of the shrinker risk. This rule can be applied with any of $\hat{\delta} = \hat{\delta}_B, \hat{\delta}_S$, or $\hat{\delta}_D$, and the risk functions are computed using the efficient RCPP integral representations discussed in Section 5.1. Unlike the standard Neyman allocation setting, the shrinker risk depends on both $\boldsymbol{\tau}$ and \mathbf{V} , so we retain updating estimates of both these quantities throughout the experiment. Notably, this means early estimates of treatment effects can directly influence future allocation decisions. Additionally, note that this algorithm is not random after we condition on all the arrivals prior to the i^{th} one.

We do not make any claims of optimality for this algorithm relative to alternative treatment rules that might also try to minimize the shrinker risk. Nonetheless, we consider this approach attractive in its simplicity, and demonstrate its utility in the sections to follow.

5.3 Simulations

We ran simulations to evaluate in which settings adaptivity based on shrinkage provides the most benefit. The simulations consist of a series of experiments where units arrive sequentially with a fixed total sample size N . There are two main choices we consider for the simulated experiments: how treatment is allocated to different treatment arms, and after the experiment is over, what estimator is used to estimate the treatment effects. For the treatment allocation approaches, we compare sequential risk-minimization for

Oracle allocations: K=12, N=1000

control-regime=low, kappa=9, shape=sparse

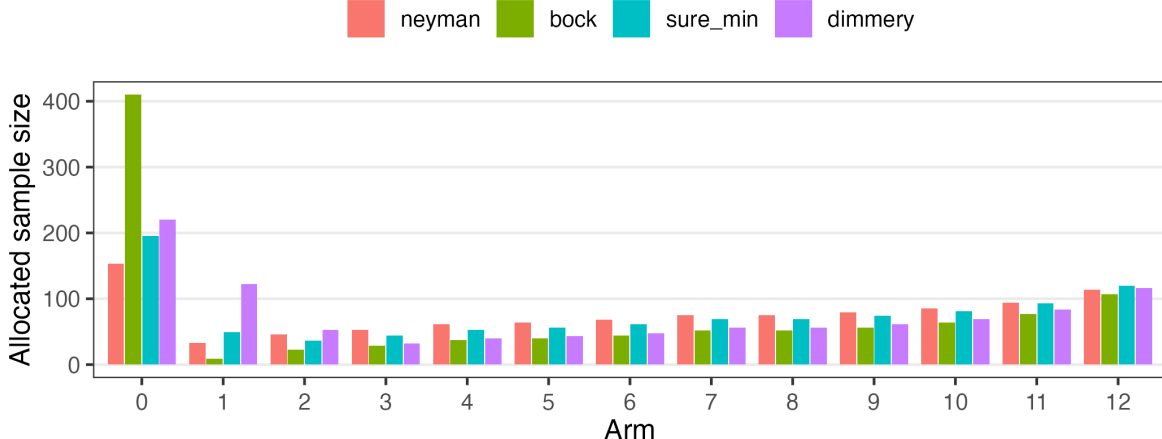


Figure 3: Oracle allocations for $K = 12$ and $N = 1,000$ with low control-variance regime, $\kappa = 9$, and sparse τ . Here, we see two key trends. First, the control reallocation for Bock’s estimator is much larger than in the otherwise-identical case in which τ is dense (Figure 2). This reflects the dependency of the minimizing allocation for Bock’s estimator on the signal density. Second, we see that the minimizing allocation for Dimmery’s estimator – but not the Bock or SURE-min estimator – tends to allocate more units to the treatment arm with strong signal when τ is sparse.

$\hat{\delta}_B$, $\hat{\delta}_S$, and $\hat{\delta}_D$ to the static allocation methods of complete randomization and Neyman allocation. For the estimators, we compare $\hat{\delta}_B$, $\hat{\delta}_S$, and $\hat{\delta}_D$ to the difference-in-means estimator $\hat{\tau}$.

To evaluate the performance, for each experiment, we calculate the mean squared error as each additional unit arrives in the trial. We then simulate repeated iterations, each time drawing a new set of potential outcomes and running a sequential experiment. After completing a set of iterations, we summarize the results by computing the average of the MSE across the simulation iterations to produce an average MSE trajectory. For detailed information about the simulation design, see Appendix G.

We highlight six regimes among the ones considered in Section 4.3. Figures 4-6 each show the trajectory of mean squared error as units arrive in trial for one simulation regime. All have $K = 6$, high control-variance, and τ sparse, but show increasing values of κ from 0 to 3 to 9. Figures 7-8 show the simulations with the same settings but τ dense for $\kappa = 3$ and $\kappa = 9$. In Appendix H, figures 9-13 show the same set of plots for the low control-variance regime.

Based on previous results, we confirm that risk-minimization treatment allocation targeting shrinkage estimators provides the greatest benefit when the signal is low and the noise is high (when the signal-to-noise ratio $\kappa = 0$ or $\kappa = 3$). In all of our settings, risk-minimization targeting Bock’s estimator does not provide substantial benefit over Neyman allocation. Empirically, it may be difficult to find a setting where Bock’s estimator dominates the difference-in-means estimator. At the largest $\kappa = 9$, risk-minimization targeting Dimmery’s estimator still provides benefit while SURE-min does not, which is consistent with Dimmery’s estimator performing better at sampling more units for arms with a strong signal. The simulations also confirm that the shrinkage estimators provide the most benefit when τ is sparse; when τ is dense and $\kappa = 9$, targeting Dimmery’s estimator provides slightly worse performance compared to Neyman allocation.

Table 4 shows a summary of the performance of the different treatment allocation strategies across regimes, but only showing $K = 6$ regimes due to limits on computational time. To attempt to summarize each strategy with single-number summaries, we report two numbers: the average across simulations of the single MSE for unit 1000, and the average across simulations for the mean MSE for units from 1000 until the end of the experiment. We chose these two measures than the mean MSE across all units in the experiment because the MSE starts high at the start of the experiment and then decreases as units arrive, so the mean MSE would be mostly a function of the earlier units when performance of all strategies is not very high. For simplicity, for each treatment allocation strategy we report only the result

for the estimator that is most naturally paired with that strategy, e.g. applying Bock’s estimator to the risk-minimization treatment allocation that targets Bock’s estimator. Both complete randomization and the Neyman treatment allocation strategies are paired with the difference-in-means estimator. For each of the two metrics, the value of the lowest MSE is in bold.

Table 4 demonstrates that the risk-minimization treatment allocations targeting the SURE-min and Dimmery’s estimator provide the best performance across all regimes. Neither the non-adaptive approaches nor targeting Bock’s estimator provide the lowest MSE across any of the regimes we considered. Targeting the SURE-min estimator results in the best performance when τ is dense, while targeting Dimmery’s estimator performs better when τ is sparse. When τ is sparse, the difference between targeting the SURE-min estimator and Dimmery’s estimator is largest when $\kappa = 9$.

Table 4: Summary of simulation performance of adaptive treatment allocation strategies

K	V ₀ regime	τ shape	κ	MSE for Unit 1000					Mean MSE for Unit ≥ 1000				
				CR	Neyman	Bock	SURE-min	Dimmery	CR	Neyman	Bock	SURE-min	Dimmery
6	high	—	0	58.13	42.71	36.90	3.43	6.20	32.28	25.41	20.94	2.14	3.48
6	high	dense	3	71.61	54.13	49.50	21.23	21.45	40.47	30.77	28.39	16.98	17.37
6	high	sparse	3	46.21	33.90	30.33	7.14	7.60	26.13	18.62	17.13	5.68	5.43
6	high	dense	9	43.34	26.18	27.12	22.67	23.88	24.64	14.84	15.38	15.53	17.01
6	high	sparse	9	49.62	40.66	37.41	18.22	17.34	28.43	22.77	22.55	14.10	12.08
6	low	—	0	20.51	19.93	13.91	1.13	2.01	11.87	11.32	7.79	0.67	0.98
6	low	dense	3	17.83	16.18	13.15	5.92	6.38	10.08	9.41	7.94	4.95	5.15
6	low	sparse	3	49.25	39.46	28.79	6.66	6.11	28.51	22.64	16.79	5.07	4.29
6	low	dense	9	13.73	11.48	10.03	8.86	9.57	7.93	6.70	5.95	6.22	6.84
6	low	sparse	9	25.61	24.74	18.30	12.03	10.37	14.31	13.86	11.61	8.91	7.19

Each metric (MSE for Unit 1000 and Mean MSE for Unit ≥ 1000) is the mean across simulation iterations. For each metric, the value of the lowest MSE is in bold. CR stands for Complete Randomization.

6 Discussion

Herein, we have proposed a novel approach to adaptive experimental designs, in which our final causal estimate is obtained by applying an Empirical Bayes shrinker to the relevant contrasts between arms. We considered three sensible shrinkers for the case of heteroscedastic and dependent data: Bock’s estimator $\hat{\delta}_B$, an easy-to-compute SURE-minimizing estimator $\hat{\delta}_S$, and Dimmery’s estimator $\hat{\delta}_D$. Each admits a testable condition under which its risk is guaranteed to outperform the simple difference-in-means estimator.

Under a non-adaptive design with known true parameter values, the risk-minimizing allocations for each of these shrinkage estimators diverges from a standard Neyman allocation. Most notably, these allocations all inflate the number of units assigned to the control condition, which tends to de-correlate the causal estimates. This gives the shrinkers “more independent” data from which to learn. We also showed that these estimators can be used for sequential adaptivity, because their risks can be expressed as efficiently-computable sums of ratios of Gaussian quadratic forms. Hence, by maintaining online estimates of the mean and variance parameters and using a greedy minimization scheme, we can assign units to treatment arms in order to minimize the risk of our estimator. Simulations demonstrate that this method outperforms an adaptive Neyman allocation, particularly when the potential outcome variances are large.

There are many future directions for this research. First, our greedy algorithm – used for adaptively assigning treatments to units – is deterministic conditional on the units already observed. This makes it sensitive to unlucky observations early in the experiment. Many modern methods (Dai et al., 2023; Li and Owen, 2024, e.g.) instead allocate treatment probabilistically at each stage. These methods either gradually update treatment probabilities with each new arrival to the trial, or recompute treatment probabilities at each stage in a batched experiment. Such approaches may better manage the exploration-exploitation tradeoff than our greedy approach, and may also show faster convergence to the true optimal treatment probabilities for a given value of τ and the potential outcome variances $\{V_k\}_{k=0}^K$.

Moreover, our focus in this manuscript has been on estimation, but many practical applications will also require inferential tools. Constructing valid frequentist confidence intervals for shrinkage estimators

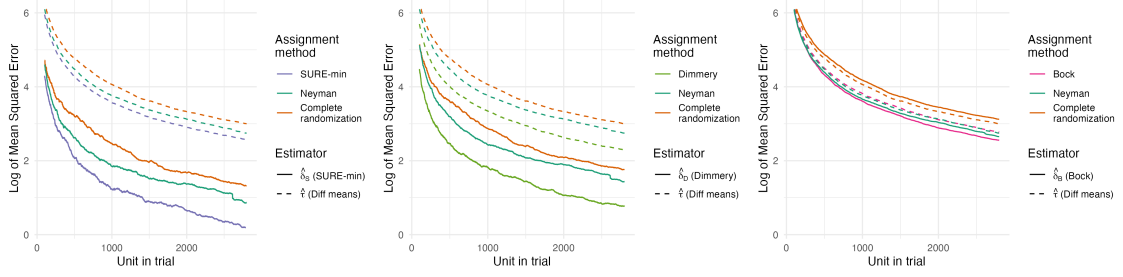


Figure 4: $\kappa = 0$.

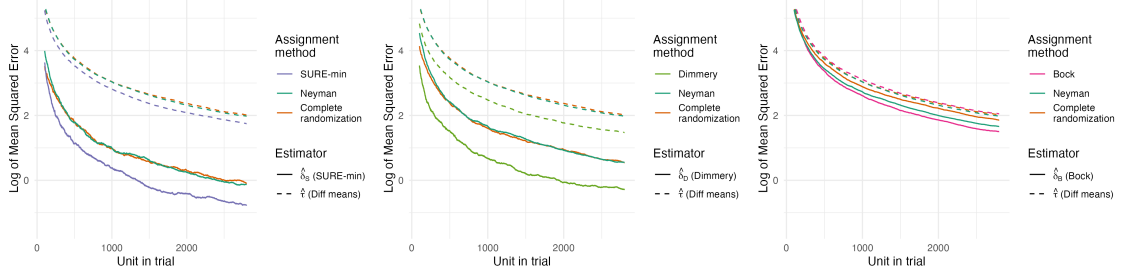


Figure 5: τ sparse, $\kappa = 3$.

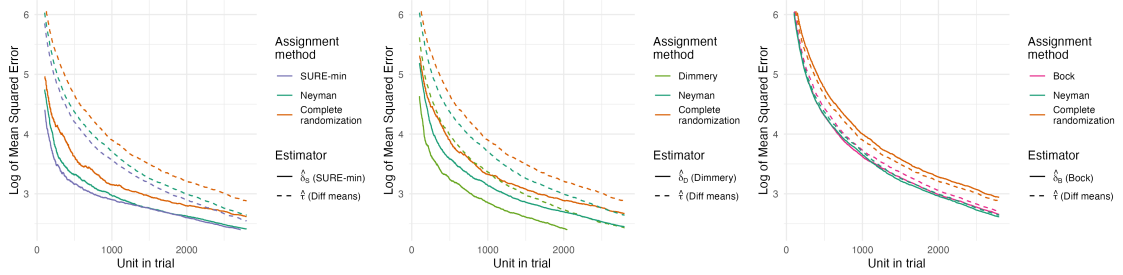


Figure 6: τ sparse, $\kappa = 9$.

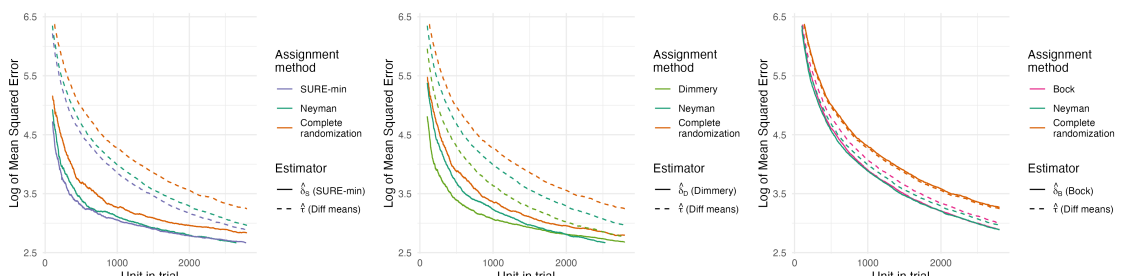


Figure 7: τ dense, $\kappa = 3$.

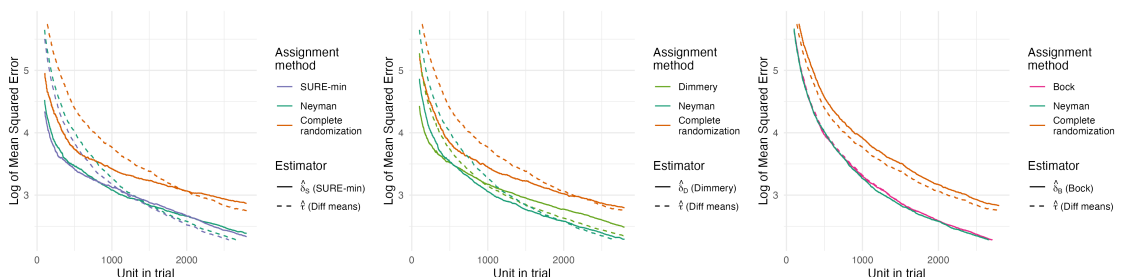


Figure 8: τ dense, $\kappa = 9$.

is an open area of research (Armstrong et al., 2022; Hoff, 2022). Some work has focused on a weaker notion of confidence interval coverage known as “Empirical Bayes coverage.” In this approach, the guarantee is not that intervals cover with a $1 - \alpha$ probability (for a user-chosen value of α), but rather than a $1 - \alpha$ fraction of the causal effects will be covered by the intervals on average. As a consequence, outlying effects may rarely be covered (Armstrong et al., 2022). Even if we were to consider this weaker notion of coverage, adaptivity poses other challenges for valid confidence interval construction, especially if the trial may be stopped at any time (Hadad et al., 2021; Maharaj et al., 2023, see e.g.). Future work should consider the potential limitations of our approach when it comes to inference. If valid frequentist intervals are needed for every causal estimand, analysts may not be able to deploy shrinkage estimators, despite their benefits for estimation.

Lastly, we have considered three reasonable estimators in this manuscript, finding that the SURE-min estimator $\hat{\delta}_S$ and Dimmery’s estimator $\hat{\delta}_D$ tend to yield improved performance in different simulation regimes. Yet our method is valid for any shrinkage estimator whose risk can be expressed as a sum of ratios of Gaussian quadratic forms. Moreover, there is a rich literature on the construction of shrinkage estimators using unbiased risk estimators in the vein of Stein’s Unbiased Risk Estimate (Li et al., 1985; Xie et al., 2012b; Donoho and Johnstone, 1995). Hence, future efforts may focus on the design of shrinkers that are specially tailored to the tasks of causal estimation in adaptive experiments. Such estimators would be especially useful if they incorporated covariates, allowing side information to further improve estimation accuracy. These advances – in tandem with practical guidance about when and where to use different candidate estimators – would help to operationalize our method and make it accessible to a broader group of practitioners.

References

S. Agrawal and N. Goyal. Analysis of Thompson sampling for the multi-armed bandit problem. *Journal of Machine Learning Research*, 23(1):1–26, 2012. URL <http://jmlr.org/papers/v23/agrawal12a.html>.

D. Arbour, D. Dimmery, and T. Mai. Online balanced experimental design. *Proceedings of the 39 th International Conference on Machine Learning*, 2022.

T. B. Armstrong, M. Kolesár, and M. Plagborg-Møller. Robust empirical bayes confidence intervals. *Econometrica*, 90(6):2567–2602, 2022.

A. C. Atkinson. Optimum biased coin designs for sequential clinical trials with prognostic factors. *Biometrika*, 69(1):61–67, 1982. doi: 10.1093/biomet/69.1.61.

Y. Bao and R. Kan. On the moments of ratios of quadratic forms in normal random variables. *Journal of Multivariate Analysis*, 117:229–245, 2013.

D. Blackwell and J. L. Hodges. Design for the control of selection bias. *Annals of Statistics*, 7(2):299–307, 1979. doi: 10.1214/aos/1176344646.

M. Blackwell, N. E. Pashley, and D. Valentino. Batch adaptive designs to improve efficiency in social science experiments. Working paper, Harvard University, 2022. URL https://www.mattblackwell.org/files/papers/batch_adaptive.pdf.

M. E. Bock. Minimax estimators of the mean of a multivariate normal distribution. *The Annals of Statistics*, pages 209–218, 1975.

J. R. Bunch, C. P. Nielsen, and D. C. Sorensen. Rank-one modification of the symmetric eigenproblem. *Numerische Mathematik*, 31(1):31–48, 1978.

Y. Cai and A. Rafi. On the performance of the neyman allocation with small pilots. *Journal of Econometrics*, 242(1):105793, 2024.

F. Chen, S. Ge, J. Qian, and C. Harshaw. Sigmoid-ftrl: Design-based adaptive neyman allocation for aipw estimators. *arXiv preprint arXiv:2511.19905*, 2025.

J. Dai, P. Gradu, and C. Harshaw. Clip-ogd: An experimental design for adaptive neyman allocation in sequential experiments. *Advances in Neural Information Processing Systems*, 36:32235–32269, 2023.

D. Dimmery, E. Bakshy, and J. Sekhon. Shrinkage estimators in online experiments. In *Proceedings of the 25th ACM SIGKDD International Conference on Knowledge Discovery & Data Mining*, pages 2914–2922, 2019.

D. L. Donoho and I. M. Johnstone. Adapting to unknown smoothness via wavelet shrinkage. *Journal of the american statistical association*, 90(432):1200–1224, 1995.

D. Eddelbuettel and R. François. Rcpp: Seamless R and C++ integration. *Journal of Statistical Software*, 40(8):1–18, 2011. doi: 10.18637/jss.v040.i08.

B. Efron. *Large-scale inference: empirical Bayes methods for estimation, testing, and prediction*. Cambridge University Press, 2012.

V. Hadad, D. A. Hirshberg, R. Zhan, S. Wager, and S. Athey. Confidence intervals for policy evaluation in adaptive experiments. *Proceedings of the national academy of sciences*, 118(15):e2014602118, 2021.

J. Hahn, K. Hirano, and D. Karlan. Adaptive experimental design using the propensity score. *Journal of Business & Economic Statistics*, 29(1):96–108, 2011.

D. W. Ham, I. Bojinov, M. Lindon, and M. Tingley. Design-based confidence sequences: A general approach to risk mitigation in online experimentation, 2023.

P. Hoff. Coverage properties of empirical bayes intervals: a discussion of “confidence intervals for non-parametric empirical bayes analysis” by ignatiadis and wager. *Journal of the American Statistical Association*, 117(539):1175–1178, 2022.

R. Johari, P. Koomen, L. Pekelis, and D. Walsh. Peeking at a/b tests: Why it matters, and what to do about it. In *Proceedings of the 23rd ACM SIGKDD International Conference on Knowledge Discovery and Data Mining*, pages 1517–1525, 2017.

M. Kasy and A. Sautmann. Adaptive treatment assignment in experiments for policy choice. *Econometrica*, 89(1):113–132, 2021.

M. Kato, T. Ishihara, J. Honda, and Y. Narita. Efficient adaptive experimental design for average treatment effect estimation. *arXiv preprint arXiv:2002.05308*, 2020.

H. H. Li and A. B. Owen. Double machine learning and design in batch adaptive experiments. *Journal of Causal Inference*, 12(1):20230068, 2024. doi: doi:10.1515/jci-2023-0068. URL <https://doi.org/10.1515/jci-2023-0068>.

K.-C. Li et al. From Stein’s unbiased risk estimates to the method of generalized cross validation. *The Annals of Statistics*, 13(4):1352–1377, 1985.

A. Maharaj, R. Sinha, D. Arbour, I. Waudby-Smith, S. Z. Liu, M. Sinha, R. Addanki, A. Ramdas, M. Garg, and V. Swaminathan. Anytime-valid confidence sequences in an enterprise a/b testing platform. In *Companion Proceedings of the ACM Web Conference 2023*, pages 396–400, 2023.

J. Neyman. On the two different aspects of the representative method: The method of stratified sampling and the method of purposive selection. *Journal of the Royal Statistical Society*, 97(4):558–625, 1934. doi: 10.2307/2342192.

M. Offer-Westort, E. H. Kennedy, and L. Miratrix. Adaptive experiments with control augmentation. *Journal of the Royal Statistical Society: Series B (Statistical Methodology)*, 83(5):1053–1079, 2021. doi: 10.1111/rssb.12491.

W. F. Rosenberger, N. Stallard, A. Ivanova, C. N. Harper, and M. L. Ricks. Optimal adaptive designs for binary response trials. *Biometrics*, 57(3):909–913, 2001.

L. Rosenzweig and M. Offer-Westort. Conversations with a concern-addressing chatbot increase covid-19 vaccination intentions among social media users in kenya and nigeria. *The Journal of Politics*, 0(ja): null, 0. doi: 10.1086/735504. URL <https://doi.org/10.1086/735504>.

D. B. Rubin. Estimating causal effects of treatments in randomized and nonrandomized studies. *Journal of Educational Psychology*, 66(5):688, 1974.

D. B. Rubin. Randomization analysis of experimental data: The fisher randomization test – comment. *Journal of the American Statistical Association*, 75(371):591–593, 1980.

D. Russo. Simple bayesian algorithms for best arm identification. In *Conference on learning theory*, pages 1417–1418. PMLR, 2016.

D. Russo, B. V. Roy, A. Kazerouni, I. Osband, and Z. Wen. A tutorial on thompson sampling. *Foundations and Trends in Machine Learning*, 11(1):1–96, 2018. doi: 10.1561/2200000070.

F. E. Satterthwaite. An approximate distribution of estimates of variance components. *Biometrics bulletin*, 2(6):110–114, 1946.

C. Stein. Inadmissibility of the usual estimator for the mean of a multivariate normal distribution. Technical report, Stanford University, Stanford, CA, 1956.

C. M. Stein. Estimation of the mean of a multivariate normal distribution. *The Annals of Statistics*, 9: 1135–1151, 1981.

W. E. Strawderman. On minimax estimation of a normal mean vector for general quadratic loss. In *Mathematical Statistics and Applications: Festschrift for Constance Van Eeden*, pages 3–14. Institute of Mathematical Statistics, 2003.

M. Tabord-Meehan. Stratification trees for adaptive randomization in randomized controlled trials. *arXiv preprint arXiv:1806.05127*, 2018.

W. R. Thompson. On the likelihood that one unknown probability exceeds another in view of the evidence of two samples. *Biometrika*, 25(3-4):285–294, 1933. doi: 10.2307/2332286.

L. Trippa, E. Q. Lee, P. Y. Wen, T. T. Batchelor, T. Cloughesy, G. Parmigiani, and B. M. Alexander. Bayesian adaptive randomized trial design for patients with recurrent glioblastoma. *Journal of Clinical Oncology*, 30(26):3258–3263, 2012. doi: 10.1200/JCO.2011.39.8420. URL <https://doi.org/10.1200/JCO.2011.39.8420>. PMID: 22649140.

S. S. Villar, J. Bowden, and J. Wason. Multi-armed bandit models for the optimal design of clinical trials: benefits and challenges. *Statistical science: a review journal of the Institute of Mathematical Statistics*, 30(2):199, 2015.

J. M. S. Wason and L. Trippa. A comparison of bayesian adaptive randomization and multi-stage designs for multi-arm clinical trials. *Statistics in Medicine*, 33(13):2206–2221, 2014. doi: <https://doi.org/10.1002/sim.6086>. URL <https://onlinelibrary.wiley.com/doi/abs/10.1002/sim.6086>.

X. Xie, S. Kou, and L. D. Brown. SURE estimates for a heteroscedastic hierarchical model. *Journal of the American Statistical Association*, 107(500):1465–1479, 2012a.

Y. Xie, J. E. Brand, and B. Jann. Estimating heterogeneous treatment effects with observational data. *Sociological Methodology*, 42(1):314–347, 2012b.

K. Zhang, L. Janson, and S. Murphy. Inference for batched bandits. *Advances in neural information processing systems*, 33:9818–9829, 2020.

J. Zhao. Adaptive neyman allocation. *arXiv preprint arXiv:2309.08808*, 2023.

A Proof of Lemma 1

Proof. The proof draws heavily from Lemma 4.1 and Theorem 4.1 in Strawderman (2003). Because Σ is full-rank and symmetric, there exists a unique orthogonal matrix \mathbf{Q} that satisfies

$$\mathbf{Q}\Sigma\mathbf{Q}^\top = \mathbf{D},$$

for $\mathbf{D} = \text{diag}(d_1, \dots, d_K)$ a diagonal matrix. Define $\mathbf{Z} = \mathbf{Q}\mathbf{X}$ (and, equivalently, $\mathbf{Q}^\top \mathbf{Z} = \mathbf{X}$) such that $\mathbf{Z} \sim \mathcal{N}(\mathbf{Q}\boldsymbol{\mu}, \mathbf{D})$. Observe:

$$\begin{aligned}\mathbb{E} \left(\|\hat{\boldsymbol{\delta}}(\mathbf{X}) - \boldsymbol{\mu}\|_2^2 \right) &= \mathbb{E} \left((\mathbf{X} - g(\mathbf{X}) - \boldsymbol{\mu})^\top (\mathbf{X} - g(\mathbf{X}) - \boldsymbol{\mu}) \right) \\ &= \mathbb{E} \left((\mathbf{Q}^\top \mathbf{Z} - g(\mathbf{Q}^\top \mathbf{Z}) - \boldsymbol{\mu})^\top (\mathbf{Q}^\top \mathbf{Z} - g(\mathbf{Q}^\top \mathbf{Z}) - \boldsymbol{\mu}) \right) \\ &= \mathbb{E} \left((\mathbf{Q}^\top \mathbf{Z} - \mathbf{Q}^\top \mathbf{Q}g(\mathbf{Q}^\top \mathbf{Z}) - \mathbf{Q}^\top \mathbf{Q}\boldsymbol{\mu})^\top (\mathbf{Q}^\top \mathbf{Z} - \mathbf{Q}^\top \mathbf{Q}g(\mathbf{Q}^\top \mathbf{Z}) - \mathbf{Q}^\top \mathbf{Q}\boldsymbol{\mu}) \right) \\ &= \mathbb{E} \left((\mathbf{Z} - \mathbf{Q}g(\mathbf{Q}^\top \mathbf{Z}) - \mathbf{Q}\boldsymbol{\mu})^\top (\mathbf{Z} - \mathbf{Q}g(\mathbf{Q}^\top \mathbf{Z}) - \mathbf{Q}\boldsymbol{\mu}) \right).\end{aligned}$$

The final line is the expected squared-error loss when estimating the mean of \mathbf{Z} using

$$\hat{\boldsymbol{\delta}}'(\mathbf{Z}) = \mathbf{Z} - f(\mathbf{Z}) \quad \text{for} \quad f(\mathbf{Z}) = \mathbf{Q}g(\mathbf{Q}^\top \mathbf{Z}),$$

where \mathbf{Z} is multivariate normal with independent components. Hence, we are back to the standard setting for using SURE. Applying SURE, we obtain

$$\begin{aligned}\mathbb{E} \left(\|\hat{\boldsymbol{\delta}}(\mathbf{X}) - \boldsymbol{\mu}\|_2^2 \right) &= \mathbb{E} \left(\|\hat{\boldsymbol{\delta}}'(\mathbf{Z}) - \mathbf{Q}\boldsymbol{\mu}\|_2^2 \right) \\ &= \text{tr}(\mathbf{D}) + \mathbb{E} \left(\|\mathbf{Q}g(\mathbf{Q}^\top \mathbf{Z})\|_2^2 - 2 \sum_{k=1}^K d_k \frac{\partial f_k(\mathbf{Z})}{\partial Z_k} \right).\end{aligned}$$

We observe immediately that $\text{tr}(\mathbf{D}) = \text{tr}(\boldsymbol{\Sigma})$ and

$$\begin{aligned}\|\mathbf{Q}g(\mathbf{Q}^\top \mathbf{Z})\|_2^2 &= g(\mathbf{Q}^\top \mathbf{Z})^\top \mathbf{Q}^\top \mathbf{Q}g(\mathbf{Q}^\top \mathbf{Z}) = g(\mathbf{Q}^\top \mathbf{Z})^\top g(\mathbf{Q}^\top \mathbf{Z}) \\ &= g(\mathbf{X})^\top g(\mathbf{X}) = \|g(\mathbf{X})\|_2^2.\end{aligned}$$

Lastly, define $\mathcal{J}_f(\mathbf{Z})$ as the Jacobian matrix of $f(\cdot)$ evaluated at \mathbf{Z} . Via the Chain Rule, we obtain

$$\begin{aligned}\sum_{k=1}^K d_k \frac{\partial f_k(\mathbf{Z})}{\partial Z_k} &= \text{tr}(\mathbf{D}\mathcal{J}_f(\mathbf{Z})) \\ &= \text{tr}(\mathbf{D}\mathbf{Q}\mathcal{J}_g(\mathbf{Q}^\top \mathbf{Z})\mathbf{Q}^\top) \\ &= \text{tr}(\mathbf{Q}^\top \mathbf{D}\mathbf{Q}\mathcal{J}_g(\mathbf{Q}^\top \mathbf{Z})) \\ &= \text{tr}(\boldsymbol{\Sigma}\mathcal{J}_g(\mathbf{X})),\end{aligned}$$

where we have used the cyclic property of the trace on the second-to-last line and the fact that $\mathbf{Q}^\top \mathbf{D}\mathbf{Q} = \boldsymbol{\Sigma}$ and $\mathbf{Q}^\top \mathbf{Z} = \mathbf{X}$ on the final line. \square

B Proof of Lemma 2

Proof. We compute the risk of $\hat{\boldsymbol{\delta}}_S$ using Expression 1:

$$\begin{aligned}\mathcal{R} \left(\hat{\boldsymbol{\delta}}_S, \boldsymbol{\tau} \right) &= \text{tr}(\boldsymbol{\Sigma}) + \mathbb{E} \left(\frac{\text{tr}(\boldsymbol{\Sigma})^2}{\|\hat{\boldsymbol{\tau}}\|_2^2} - 2 \frac{\text{tr}(\boldsymbol{\Sigma})^2}{\|\hat{\boldsymbol{\tau}}\|_2^2} + 4 \frac{\text{tr}(\boldsymbol{\Sigma})(\hat{\boldsymbol{\tau}}^\top \boldsymbol{\Sigma} \hat{\boldsymbol{\tau}})}{\|\hat{\boldsymbol{\tau}}\|_2^4} \right) \\ &= \text{tr}(\boldsymbol{\Sigma}) + \mathbb{E} \left(-\frac{\text{tr}(\boldsymbol{\Sigma})^2}{\|\hat{\boldsymbol{\tau}}\|_2^2} + 4 \frac{\text{tr}(\boldsymbol{\Sigma})(\hat{\boldsymbol{\tau}}^\top \boldsymbol{\Sigma} \hat{\boldsymbol{\tau}})}{\|\hat{\boldsymbol{\tau}}\|_2^4} \right) \\ &\leq \text{tr}(\boldsymbol{\Sigma}) + \mathbb{E} \left(\frac{4 \cdot \text{tr}(\boldsymbol{\Sigma}) \cdot \lambda_{\max}(\boldsymbol{\Sigma})}{\|\hat{\boldsymbol{\tau}}\|_2^2} - \frac{\text{tr}(\boldsymbol{\Sigma})^2}{\|\hat{\boldsymbol{\tau}}\|_2^2} \right) \\ &= \text{tr}(\boldsymbol{\Sigma}) + \text{tr}(\boldsymbol{\Sigma}) \cdot \mathbb{E} \left(\frac{4 \cdot \lambda_{\max}(\boldsymbol{\Sigma}) - \text{tr}(\boldsymbol{\Sigma})}{\|\hat{\boldsymbol{\tau}}\|_2^2} \right).\end{aligned}$$

We know that $\mathcal{R}(\hat{\boldsymbol{\tau}}, \boldsymbol{\tau}) = \text{tr}(\boldsymbol{\Sigma})$, so $\hat{\boldsymbol{\delta}}_S$ dominates $\hat{\boldsymbol{\tau}}$ if the expectation term is negative, which occurs precisely when the given condition holds. \square

C Proof of Lemma 3

Proof. From Expression 1, we can directly compute the risk of $\hat{\delta}_D$. Denote as Σ_* the diagonal matrix whose diagonal entries are equal to the diagonal entries of Σ . Then, we obtain

$$\begin{aligned}\mathcal{R}(\hat{\delta}_D, \tau) &= \text{tr}(\Sigma) + \mathbb{E} \left(\frac{(K-2)^2}{\|\hat{\tau}\|_2^4} (\hat{\tau}^\top \Sigma \Sigma_*^2 \hat{\tau}) + \frac{4(K-2)}{\|\hat{\tau}\|_2^4} (\hat{\tau}^\top \Sigma \Sigma_* \hat{\tau}) - \frac{2(K-2)\text{tr}(\Sigma_*^2)}{\|\hat{\tau}\|_2^2} \right) \\ &\leq \text{tr}(\Sigma) + (K-2)\mathbb{E} \left(\frac{4\hat{\tau}^\top \Sigma \Sigma_* \hat{\tau}}{\|\hat{\tau}\|_2^4} + \frac{(K-2) \max_k \sigma_k^4 - 2 \cdot \text{tr}(\Sigma_*^2)}{\|\hat{\tau}\|_2^2} \right)\end{aligned}$$

We bound the first quadratic form directly. For any vector $\hat{\tau}$,

$$\begin{aligned}\hat{\tau}^\top \Sigma \Sigma_* \hat{\tau} &= \hat{\tau}^\top \Sigma (\Sigma_* \hat{\tau}) \\ &\leq \|\hat{\tau}\|_2 \|\Sigma (\Sigma_* \hat{\tau})\|_2 \\ &\leq \|\hat{\tau}\|_2 \lambda_{\max}(\Sigma) \|\Sigma_* \hat{\tau}\|_2 \\ &\leq \lambda_{\max}(\Sigma) (\max_k \sigma_k^2) \|\hat{\tau}\|_2^2.\end{aligned}$$

Plugging this in, we obtain

$$\mathcal{R}(\hat{\delta}_D, \tau) \leq \text{tr}(\Sigma) + (K-2)\mathbb{E} \left(\frac{4\lambda_{\max}(\Sigma) (\max_k \sigma_k^2) + (K-2) \max_k \sigma_k^4 - 2 \cdot \text{tr}(\Sigma_*^2)}{\|\hat{\tau}\|_2^2} \right)$$

If the numerator is negative, then $\hat{\delta}_D$ dominates $\hat{\tau}$. This yields precisely the given condition. \square

D Proof of Lemma 4

Proof. The objective is convex, and an equal allocation is one example of a feasible interior point satisfying Slater's condition. Hence, we can use the standard approach of Lagrange Multipliers to find the optimum. The Lagrangian is given by

$$\mathcal{L}(n_0, \dots, n_K) = \frac{KV_0}{n_0} + \sum_{k=1}^K \frac{V_k}{n_k} + \lambda \left(\sum_{k=0}^K n_k - N \right),$$

with derivatives

$$\begin{aligned}\frac{\partial \mathcal{L}(n_0, \dots, n_K)}{\partial n_0} &= -\frac{KV_0}{n_0^2} + \lambda, \\ \frac{\partial \mathcal{L}(n_0, \dots, n_K)}{\partial n_k} &= -\frac{V_k}{n_k^2} + \lambda, \quad k = 1, \dots, K \\ \frac{\partial \mathcal{L}(n_0, \dots, n_K)}{\partial \lambda} &= \sum_{k=0}^K n_k - N.\end{aligned}$$

Setting these derivatives equal to 0, we obtain

$$\lambda = \frac{KV_0}{n_0^2} = \frac{V_1}{n_1^2} = \dots = \frac{V_K}{n_K^2}. \tag{18}$$

This implies that

$$\sum_{k=0}^K n_k = \frac{1}{\sqrt{\lambda}} \left(\sqrt{KV_0} + \sum_{k=1}^K \sqrt{V_k} \right) = N.$$

from which the result directly follows. \square

E Proof of Lemma 5

Proof. Applying Lemma 1,

$$\begin{aligned}\mathcal{R}(\hat{\delta}_B, \tau) &= \text{tr}(\Sigma) + \mathbb{E} \left(\frac{(\tilde{p}-2)^2 \|\hat{\tau}\|_2^2}{(\hat{\tau}^\top \Sigma^{-1} \hat{\tau})^2} - \frac{2(\tilde{p}-2)}{\hat{\tau}^\top \Sigma^{-1} \hat{\tau}} \text{tr}(\Sigma) + \frac{4(\tilde{p}-2) \|\hat{\tau}\|_2^2}{(\hat{\tau}^\top \Sigma^{-1} \hat{\tau})^2} \right) \\ &= \text{tr}(\Sigma) + (\tilde{p}^2 - 4) \mathbb{E} \left(\frac{\|\hat{\tau}\|_2^2}{(\hat{\tau}^\top \Sigma^{-1} \hat{\tau})^2} \right) - 2(\tilde{p}-2) \text{tr}(\Sigma) \mathbb{E} \left(\frac{1}{\hat{\tau}^\top \Sigma^{-1} \hat{\tau}} \right).\end{aligned}\tag{19}$$

If $\|\tau\|_2^2 = 0$, then $\hat{\tau} \sim \mathcal{N}(\mathbf{0}, \Sigma)$. Define $Z = \Sigma^{-1/2} \hat{\tau}$, so $Z \sim \mathcal{N}(\mathbf{0}, I)$. Then

$$(\hat{\tau}^\top \Sigma^{-1} \hat{\tau}) = \|Z\|_2^2 \sim \chi_K^2.$$

The inverse- χ^2 moment yields

$$\mathbb{E} \left(\frac{1}{\hat{\tau}^\top \Sigma^{-1} \hat{\tau}} \right) = \frac{1}{K-2}.$$

To evaluate the remaining term, observe

$$\frac{\|\hat{\tau}\|_2^2}{(\hat{\tau}^\top \Sigma^{-1} \hat{\tau})^2} = \frac{Z^\top \Sigma X}{\|Z\|_2^4} = \frac{\|Z\|_2^2 \cdot U^\top \Sigma U}{\|Z\|_2^4} = \frac{U^\top \Sigma U}{\|Z\|_2^2}$$

where $U = Z/\|Z\|_2$, such that U is uniform on the unit sphere and independent of $\|Z\|_2$.

By symmetry, $\mathbb{E}(U^\top \Sigma U) = \text{tr}(\Sigma)/K$. Applying independence and the prior result, we obtain

$$\mathbb{E} \left(\frac{\|\hat{\tau}\|_2^2}{(\hat{\tau}^\top \Sigma^{-1} \hat{\tau})^2} \right) = \frac{\text{tr}(\Sigma)}{K(K-2)}.$$

Plugging these identities into Equation 19 yields the given risk. \square

F Proof of Lemma 6

Proof. Denote as Σ_{NA} the covariance matrix of $\hat{\tau}$ at the Neyman allocation, which is given by

$$\Sigma_{NA} = S_{NA} \left(\text{diag}(\sqrt{V_1}, \dots, \sqrt{V_K}) + \sqrt{\frac{V_0}{K}} \mathbb{1} \mathbb{1}^\top \right), \tag{20}$$

where

$$S_{NA} = \frac{1}{N} \left(\sqrt{KV_0} + \sum_{\ell=1}^K \sqrt{V_\ell} \right).$$

Moreover, by the Bunch-Nielsen-Sorensen formula (Bunch et al., 1978), the dominant eigenvector ν_{NA} will have k^{th} entry proportional to $(\lambda_{\max}(\Sigma) - \sqrt{V_k})^{-1}$. Moreover, we see

$$\text{tr}(\Sigma_{NA}) = S_{NA} \left(\sqrt{KV_0} + \sum_{\ell=1}^K \sqrt{V_\ell} \right) = NS_{NA}^2.$$

Lastly, denote as $\nu_{NA} = (\nu_1, \dots, \nu_K)^\top$ the dominant eigenvector associated with $\lambda_{\max}(\Sigma_{NA})$, scaled such that $\|\nu_{NA}\|_2^2 = 1$.

We begin by computing the relevant derivatives at the Neyman allocation.

$$\frac{\partial \tilde{p}}{\partial n_0} = \frac{KV_0}{n_0^2} \frac{\frac{\text{tr}(\Sigma)}{K} (\mathbb{1}^\top \nu_{NA})^2 - \lambda_{\max}(\Sigma)}{\lambda_{\max}(\Sigma)^2} \quad \text{and} \quad \frac{\partial \tilde{p}}{\partial n_k} = \frac{V_k}{n_k^2} \frac{\text{tr}(\Sigma) \nu_k^2 - \lambda_{\max}(\Sigma)}{\lambda_{\max}(\Sigma)^2}, \quad k = 1, \dots, K.$$

We also know that, at the Neyman allocation,

$$\frac{KV_0}{n_0^2} = \frac{V_1}{n_1^2} = \dots = \frac{V_K}{n_K^2}$$

(see the Appendix, Section D for more details). Hence, the derivative in n_0 will exceed all the other derivatives if

$$\frac{(\mathbb{1}^\top \nu_{NA})^2}{K} \geq \nu_k^2 \quad \text{for all } k = 1, \dots, K. \tag{21}$$

We also know that the covariance matrix of $\hat{\tau}$ satisfies

$$\Sigma_{\mathbf{NA}} \propto \text{diag} \left(\sqrt{V_1}, \dots, \sqrt{V_K} \right) + \sqrt{\frac{V_0}{K}} \mathbb{1} \mathbb{1}^\top.$$

Standard results for the eigenvalues of a diagonal matrix plus a rank-one update yield the following bounds on $\lambda_{\max}(\Sigma_{\mathbf{NA}})$:

$$\sqrt{KV_0} + \frac{1}{K} \sum_{k=1}^K \sqrt{V_k} \leq \lambda_{\max}(\Sigma_{\mathbf{NA}}) \leq \sqrt{KV_0} + \max_{k \geq 1} \sqrt{V_k}.$$

Moreover, by the Bunch-Nielsen-Sorensen formula (Bunch et al., 1978), the dominant eigenvector $\nu_{\mathbf{NA}}$ will have k^{th} entry proportional to $(\lambda_{\max}(\Sigma) - \sqrt{V_k})^{-1}$.

Under the heteroscedasticity condition on the potential outcomes (Condition 8) we have

$$\left(\max_{k \geq 1} \sqrt{V_k} - \min_{k \geq 1} \sqrt{V_k} \right) \leq \frac{1}{2} \sqrt{KV_0},$$

Condition 8 induces a simple bound on the ratio between the largest and smallest entries of $\nu_{\mathbf{NA}}$:

$$\begin{aligned} \frac{\max_k \nu_k}{\min_k \nu_k} &= \frac{\lambda_{\max}(\Sigma) - \min_{k \geq 1} \sqrt{V_k}}{\lambda_{\max}(\Sigma) - \max_{k \geq 1} \sqrt{V_k}} = 1 + \frac{\max_{k \geq 1} \sqrt{V_k} - \min_{k \geq 1} \sqrt{V_k}}{\lambda_{\max}(\Sigma) - \max_{k \geq 1} \sqrt{V_k}} \\ &\leq 1 + \frac{\frac{1}{2} \sqrt{KV_0}}{\sqrt{KV_0} + \left(\frac{1}{K} \sum_{k=1}^K \sqrt{V_k} - \max_{k \geq 1} \sqrt{V_k} \right)} \\ &\leq 1 + \frac{\frac{1}{2} \sqrt{KV_0}}{\sqrt{KV_0} + \left(\min_{k \geq 1} \sqrt{V_k} - \max_{k \geq 1} \sqrt{V_k} \right)} \\ &\leq 1 + \frac{\frac{1}{2} \sqrt{KV_0}}{\sqrt{KV_0} - \frac{1}{2} \sqrt{KV_0}} = 2. \end{aligned}$$

If the entries of the dominant eigenvector $\nu_{\mathbf{NA}}$ cannot vary by more than a factor of 2, this implies:

$$\begin{aligned} \frac{(\mathbb{1}^T \nu_{\mathbf{NA}})^2}{K} &\geq \frac{1}{K} \left((K-1) \min_k \nu_k + \max_k \nu_k \right)^2 \\ &\geq \frac{1}{K} \left(\frac{K-1}{2} \max_k \nu_k + \max_k \nu_k \right)^2 \\ &= \frac{1}{K} \left(\frac{K+1}{2} \max_k \nu_k \right)^2 \\ &= \frac{(K+1)^2}{4K} \max_k \nu_k^2 \\ &\geq \max_k \nu_k^2, \end{aligned}$$

where the last line follows from the fact that the minimizing value of $(K+1)^2/4K$ over the positive integers is 1. Hence, this directly implies Condition 21.

Hence, we have shown that if $\tau = \mathbf{0}$ and Condition 8 holds, most "efficient" way to increase \tilde{p} at the Neyman allocation is to allocate more units to the control arm. \square

G Simulation design

An **Experiment** is a fixed regime of simulation parameters. Within each **experiment**, run multiple **iterations**, where each **iteration** has a particular set of fixed potential outcomes.

Assume the following data-generating process:

- μ_0 is the mean of the control treatment arm.
- τ is the vector of treatment effects, $\{\tau_1, \dots, \tau_K\}$.

- Then $\mu = \mu_0 + \tau = \begin{pmatrix} \mu_0 \\ \mu_0 + \tau_1 \\ \vdots \\ \mu_0 + \tau_K \end{pmatrix}$ is the vector of potential outcome means.

- V_0 is the variance of the control treatment arm, and V_1, \dots, V_K are the variances of the active treatment arms.
- Ω is a $K \times K$ diagonal matrix and is the true covariance of the potential outcomes, and is a function of the variances V_0, \dots, V_K . We assume $\text{Cov}(\mathbf{Y}_i, \mathbf{Y}_j) = 0$.
- Define $\mathbf{Y}_i = \{Y_i(0), Y_i(1), \dots, Y_i(K)\}$ is the vector of potential outcomes for unit i .

Then the potential outcomes for each unit \mathbf{Y}_i are generated:

$$\mathbf{Y}_i \sim N_{K+1}(\boldsymbol{\mu}, \Omega)$$

For each **Experiment**, set fixed the data-generating process for the potential outcomes. The DGP is based on whether τ is sparse or dense, the control-variance regime, and the signal-to-noise ratio κ .

- K : number of *active* treatments. Total number of arms = $K + 1$ (K active arms + 1 control arm).
- τ : the K -vector of treatment effects. When combined with μ_0 , the mean of the control treatment arm, this implies a particular μ ($K + 1$ vector of arm means).
- Ω : true covariance of potential outcomes.
- N : number of observations in one iteration.

Also set fixed the sequential experimental design procedure:

- b_1 : batch size. How many observations are used to get initial estimates of mean and variance before risk minimization or other adaptive algorithm starts up.
- Choose a risk function, from the following options: Stein min, Bock, Dimmery, Neyman. Alternatively, you can follow complete randomization, where instead of minimizing the risk at each step, you just sequentially iterate through the different treatment arms. TODO explain Neyman.
- Choose a list of estimators, from the following options: difference in means, Stein min, Bock, Dimmery.

Finally, fix **n_iters**, the number of iterations for the experiment.

Note that there are two components that can be chosen independently: the risk function, and the estimator. For example, you could do sequential assignment using the Bock risk function, but then after the experiment is over, you could estimate the treatment effects without shrinkage using the difference-in-means estimator.

Within each **Iteration**:

- Generate \mathbf{Y} , the matrix of potential outcomes, a $N \times (K + 1)$ matrix.
- At each step $i = 1, \dots, N$
 - If $i \leq b_1$, then assign W_i sequentially.
 - If $i > b_1$, then:
 - * Estimate the running mean of each arm, $\hat{\mu}_{k,i}$ for $k = 0, \dots, K$ (e.g. running mean includes observations up to $i - 1$).
 - * Estimate the running variance of each arm, $\hat{V}_{k,i}$ for $k = 0, \dots, K$.
 - * Estimate the running treatment effects using the difference-in-means estimator, $\hat{\tau}_i$.
 - * Estimate the running covariance matrix of the treatment effects, $\hat{\Sigma}_i$.
 - * Using the chosen risk function for the experiment, calculate what the estimated risk would be if the next unit were to be assigned to each arm. Define $\hat{\mathcal{R}}_{k,i}$ as the risk if the next unit i is assigned to arm k . Recall that the risk $\hat{\mathcal{R}}_{k,i}$ is the average expected loss over all arms. Calculate $\hat{\mathcal{R}}_{k,i}$ for $k = 0, \dots, K$ (using $\hat{\tau}_i$ and $\hat{\Sigma}_i$).
 - * Choose the arm with the smallest risk $\hat{\mathcal{R}}_{k,i}$ and assign $W_i = \underset{k \in 0, \dots, K}{\text{argmin}} \hat{\mathcal{R}}_{k,i}$.
 - * Record the outcome $Y_i^{obs} = Y_i(W_i)$.
- At the end of the iteration, we now have:
 - An N -vector of observed outcomes \mathbf{Y}^{obs} .
 - An N -vector of allocated treatments \mathbf{W} .
 - An list of N values of $\hat{\tau}_i$ and $\hat{\Sigma}_i$.

To evaluate the experiment:

- First evaluate each iteration:
 - For each step i , compute the vector of K MSE values of each estimator. For example, the MSE for $\hat{\delta}_{B,i}$ is $(\hat{\delta}_{B,k,i} - \tau_k)^2$ for $k = 1, \dots, K$.
 - For each step i , calculate the “compound” MSE, which is the sum of the K MSE values.
 - Track trajectories of compound MSE as units arrive.
- Across iterations:
 - Calculate the “mean trajectory” by averaging the compound MSE values across iterations, for each unit.
 - We now have the average compound MSE for each estimator for each unit.
 - Then we plot the trajectories for each estimator.

Finally, we plot multiple experiments, with the same parameter DGP but different risk functions, on the same panel of plots, to evaluate which risk function and estimators produced the lowest MSE.

H Additional simulation results

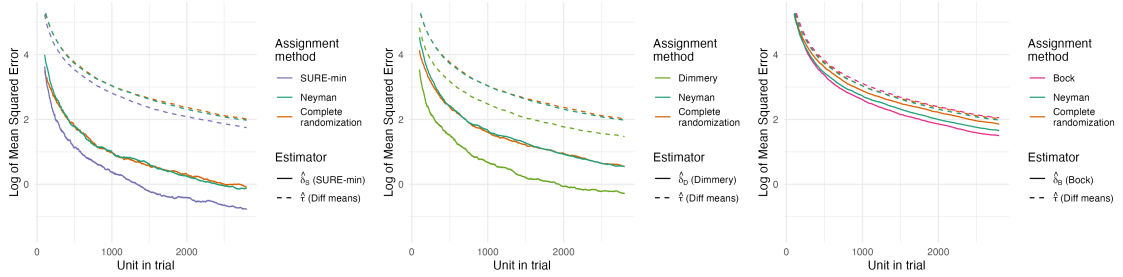


Figure 9: Low-variance control regime, $\kappa = 0$.

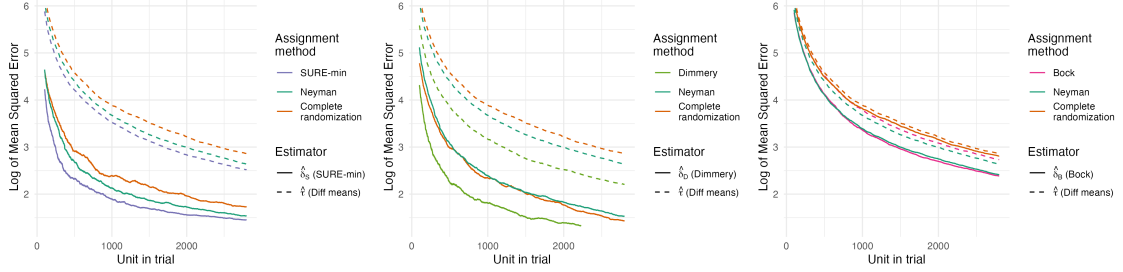


Figure 10: Low-variance control regime, τ sparse, $\kappa = 3$.

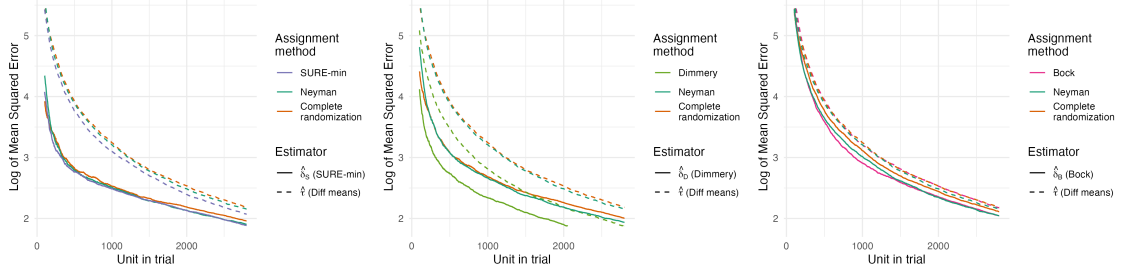


Figure 11: Low-variance control regime, τ sparse, $\kappa = 9$.

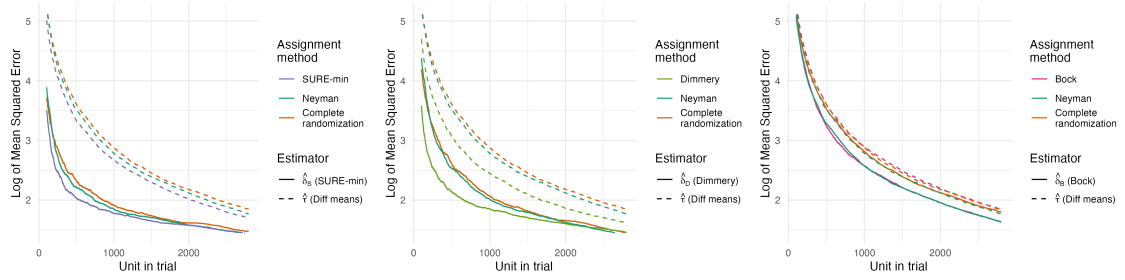


Figure 12: Low-variance control regime, τ dense, $\kappa = 3$.

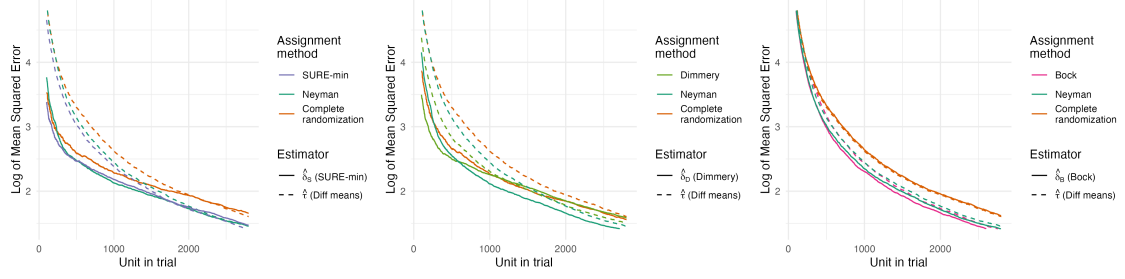


Figure 13: Low-variance control regime, τ dense, $\kappa = 9$.